Nano Research

Open Access

Review Article

Revolutionizing photothermal CO_2 hydrogenation with ceria-based catalysts

Zhaorui Zhang[1], Xiao Han[1], Junhong Zhang[1] ✉, Yunyun Dong[1], Jinsheng Zhao[1] ✉, Qian Xu[3], and Ningqiang Zhang[2] ✉

[1] *School of Chemistry and Chemical Engineering, Liaocheng University, Liaocheng 252059, China*
[2] *Institute for Catalysis, Hokkaido University, N-21, W-10, Sapporo 001-0021, Japan*
[3] *National Synchrotron Radiation Laboratory, University of Science and Technology of China, Hefei 230029, China*

Cite this article: *Nano Research*, **2025**, *18*, 94906998. https://doi.org/10.26599/NR.2025.94906998

ABSTRACT: In the context of achieving carbon neutrality, CO_2 catalytic conversion technologies are effective in reducing atmospheric CO_2 concentrations while simultaneously producing renewable products. This approach is seen as a viable method for constructing a new carbon cycle, thereby effectively addressing the issue of global warming. Photothermal CO_2 conversion has recently emerged as a promising research focus due to its high energy utilization efficiency, superior CO_2 conversion, excellent product selectivity, mild operating conditions, low energy consumption and minimal operating costs. Cerium oxide (CeO_2) has been widely used in photothermal catalysis due to its unique chemical properties, particularly when used as a support material with supported metals, creating distinctive interfacial sites for catalytic reactions. As an emerging star support in photothermal CO_2 conversion, its contributions are equally significant and should not be overlooked. However, to our knowledge, there has been no comprehensive review of CeO_2 applications in catalytic hydrogenation of CO_2. In this paper, we summarize and discuss CeO_2-based materials for photothermal CO_2 conversion to value-added products. This research particularly focuses on the synthesis methods of CeO_2-supported catalysts, the history of CeO_2 in photothermal catalysis, types of photothermal catalytic reactors, unique characterization methods for the photothermal catalysts and the photothermal CO_2 hydrogenation reactions by CeO_2-based catalysts. Perspectives related to further challenges and future directions for photothermal CO_2 hydrogenation are also provided.

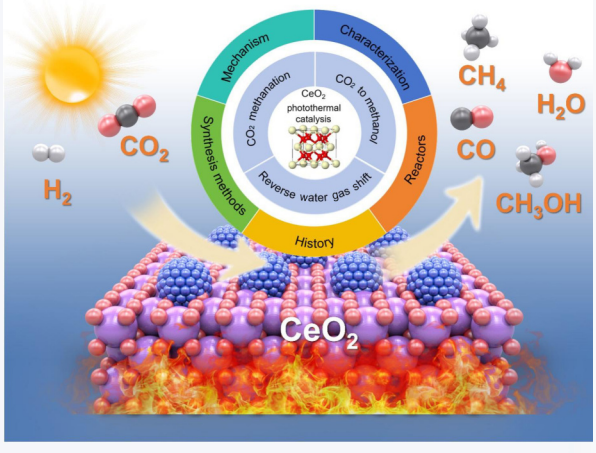

KEYWORDS: CO_2 neutrality, hydrogenation, photothermal catalysis, ceria, C1 chemistry

1 Introduction

The greenhouse effect and consequent global environmental challenges stem from the rising atmospheric carbon dioxide (CO_2) emissions resulting from fossil fuel combustion [1–8]. The as-emitted CO_2 contributes to global warming, climate anomalies, ocean storms and desertification. Therefore, addressing CO_2 emissions and their rational utilization have become central to solving environmental issues [9]. The Emissions Gap Report 2023: Broken Record—Temperatures (*T*) hit new highs, yet world fails to cut emissions (again) indicates that current climate pledges put the earth on a trajectory to warm by 2.5–2.9 °C this century, far exceeding the goals set in the Paris Agreement [10]. To limit global warming to below 1.5 °C by 2030, greenhouse gas emissions must decrease by 42%. In light of global warming, numerous countries have collaboratively set carbon neutrality objectives. Carbon capture, utilization and storage (CCUS) is an innovative technology with the potential to combat the challenge significantly [11–16]. CO_2 can be captured from emission sources, such as power plants and industries, as well as from the atmosphere and utilized as a feedstock for chemical synthesis or permanent storage by injecting

Received: July 10, 2024; **Revised:** August 11, 2024
Accepted: August 17, 2024

✉Address correspondence to Junhong Zhang, zhangjunhong@lcu.edu.cn; Jinsheng Zhao, J.S.Zhao@163.com; Ningqiang Zhang, NingqiangZhang@cat.hokudai.ac.jp

it into deep subsurface formations [17–19]. The most crucial step in CCUS is the transformation of CO_2 into renewable energy, also recognized as an effective approach to attain carbon neutrality amid the era of global carbon neutrality [20–22]. However, CO_2 represents the most oxidized form of carbon, characterized by high thermodynamic stability and kinetic inertness [23–25]. Consequently, chemical conversion of CO_2 necessitates highly reactive substrates with abundant energy, or the formation of highly stable products, often requiring more challenging reaction conditions. Therefore, conventional thermal catalytic reaction for CO_2 reduction usually operates under harsh conditions, such as high temperature and pressure [26]. Thermal catalysis involves the acceleration of chemical reactions by using a catalyst and applying heat. The catalyst provides an alternative reaction pathway with a lower activation energy, making the reaction proceed faster [27]. In the context of a low-carbon energy economy, renewable energy-driven CO_2 conversion methods, such as electrochemical and photochemical conversion, have rapidly attracted much attentions [28–32]. In photocatalysis, when the catalyst absorbs photons, electrons are excited from the valence band (VB) to the conduction band (CB), creating photogenerated electrons in the CB and leaving holes in the VB. These charge carriers drive the photocatalytic reaction. The positions of the VB and CB are critical in determining the redox potential of the photogenerated electrons and holes. A more negative CB position enhances the reducing power of the electrons, while a more positive VB position increases the oxidizing power of the holes. For CO_2 hydrogenation, the CB must be sufficiently negative to reduce CO_2 (e.g., to CO or CH_4). The energy band positions of some catalysts are shown in Fig. 1.

However, limitations related to mass transfer, catalyst degradation, adsorption of impurities and other factors have hindered the industrial application of electrochemical and photochemical CO_2 conversion [37, 38]. Although CO_2 transformation by thermal catalysis requires relatively harsh conditions, it still holds more promise than electrochemical and photochemical conversion [39, 40]. Consequently, electrothermal catalysis, photothermal catalysis and plasma-thermal catalysis have rapidly emerged in recent years [41–46]. These externally driven thermal catalysis processes can overcome the stringent conditions of traditional thermal catalysis. These driven thermal catalysis processes offer a smaller device size, facilitate easier and faster temperature management and significantly enhance CO_2 conversion efficiency, potentially surpassing the equilibrium conversion rates of traditional thermal catalysis [47–49]. Photothermal catalysis is the catalysis with the participation of both thermal and photo energies [50], heat addresses the bottleneck issues of low catalytic efficiency and limited energy-mass transfer in photocatalysis, providing the required energy to overcome the activation energy barrier. This synergy breaks through kinetic limitations, significantly enhancing catalytic activity [51, 52]. Therefore, the photothermal catalytic CO_2 reduction holds a promising research potential and application value [53–55].

Cerium dioxide (CeO_2) is widely used in heterogeneous catalysis, especially in automobile exhaust purification and catalytic CO_2 reduction, due to its excellent redox performance and oxygen

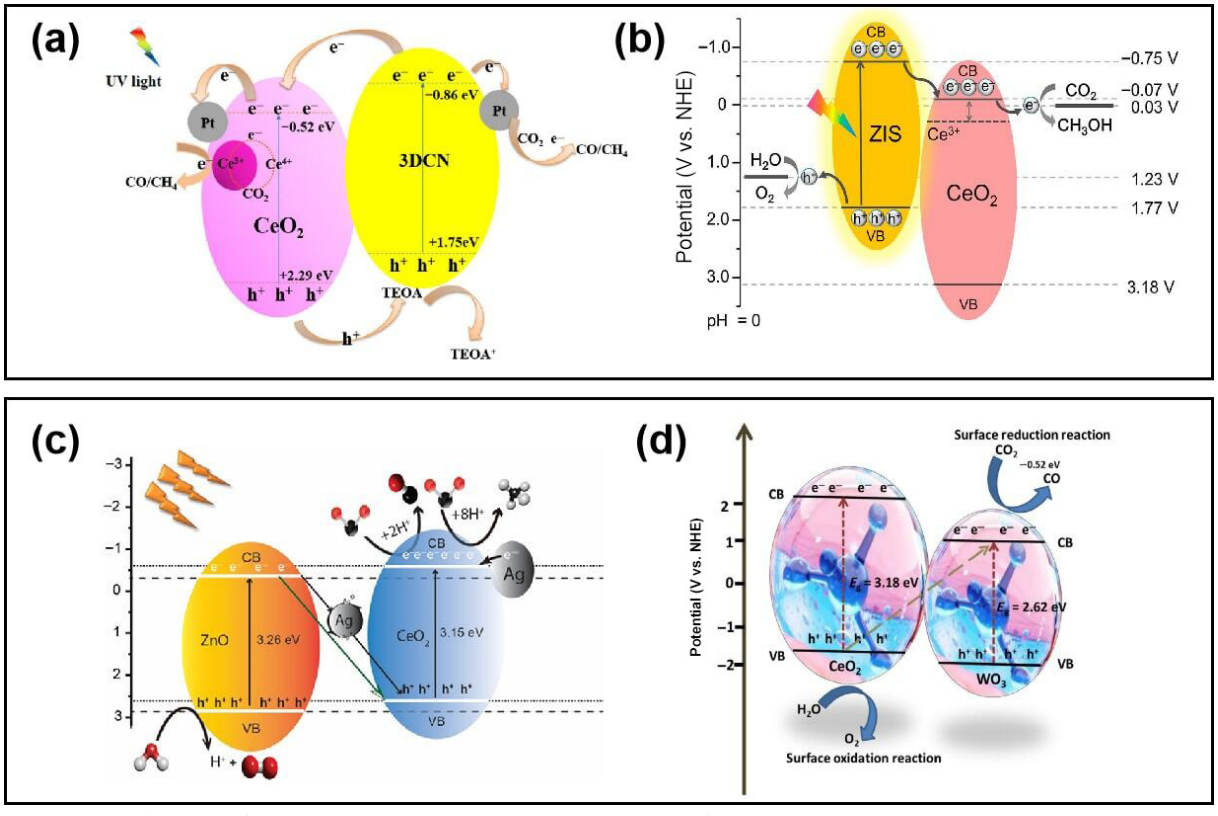

Figure 1 (a) Schematic illustration of Pt@45CeO_2/three-dimensional porous g-C_3N_4 (3DCN) for CO_2 photoconversion under UV-light irradiation. Reproduced with permission from Ref. [33], © Elsevier B.V. 2020. (b) Scheme illustrating the photocatalytic CO_2 reduction mechanism over the CeO_2/$ZnIn_2S_4$ composite. Reproduced with permission from Ref. [34], © Elsevier B.V. 2018. (c) Photocatalytic schematic mechanism of Z-scheme 3AgCZ and the probable charge separation. Reproduced with permission from Ref. [35], © American Chemical Society 2021. (d) Schematic representation of reaction mechanism for Z-scheme heterojunction. Reproduced with permission from Ref. [36], © Elsevier B.V. 2023.

storage capacity [56–67]. Additionally, its ultraviolet (UV) absorption ability, high refractive index and other optical properties have garnered significant attention for applications in photothermal CO_2 conversion [68–70].

Ce^{4+} within CeO_2 can readily convert into stable Ce^{3+} and undergo reversible switching in the oxidation-reduction cycle. The resulting Ce^{3+} species can directly activate CO_2, extract oxygen from it and generate CO or carbon-containing intermediates. Additionally, when supporting metals, cerium oxide facilitates the generation of highly dispersed metal particles, increasing the interfaces between metals and cerium oxide, enhance CO_2 hydrogenation catalytic activities.

Over the past decade, there has been a burgeoning interest in photothermal catalysis [23, 29, 53, 71–75]. The field of "photothermal catalysis" has seen over 1000 publications from 2008 to 2023, reflecting a steady increase in interest over the years (Fig. 2(a)). Since 2015, the application of CeO_2-based catalysts in photothermal catalysis has also increased each year (Fig. 2(b)).

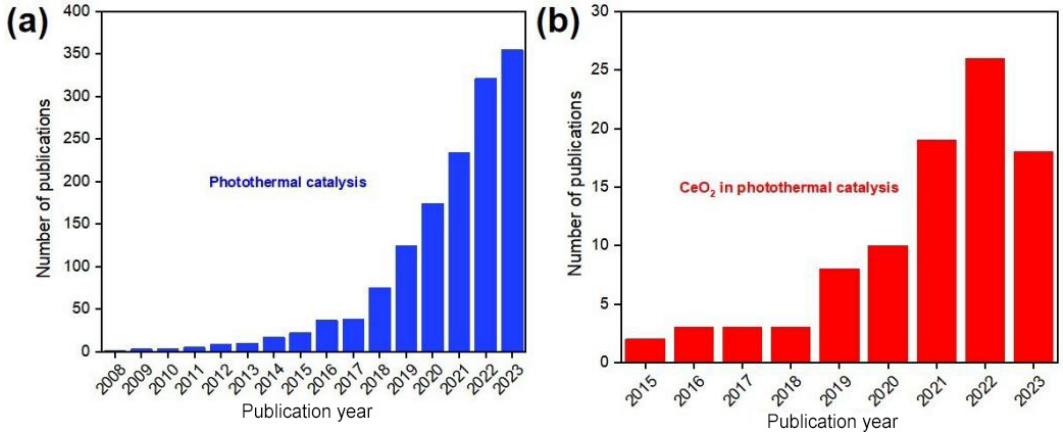

Figure 2 Number of published papers searched using (a) "photothermal catalysis" and (b) "photothermal catalysis" and "CeO_2" as keywords, from 2008 to 2023 and 2015 to 2023, respectively.

Although CeO_2 has begun to emerge in photothermal catalysis, to the best of our knowledge, a systematic overview of CeO_2 for photothermal CO_2 reactions has not yet been reported and the understanding of its mechanisms remains superficial. In this brief review, we systematically summarize the progress of CeO_2-based catalysts in photothermal CO_2 conversion. We also discuss the synthesis methods of CeO_2-supported catalysts and the characterization techniques used in mechanistic studies. Moreover, a perspective is presented on the future development of CeO_2 in this field, as illustrated in Fig. 3.

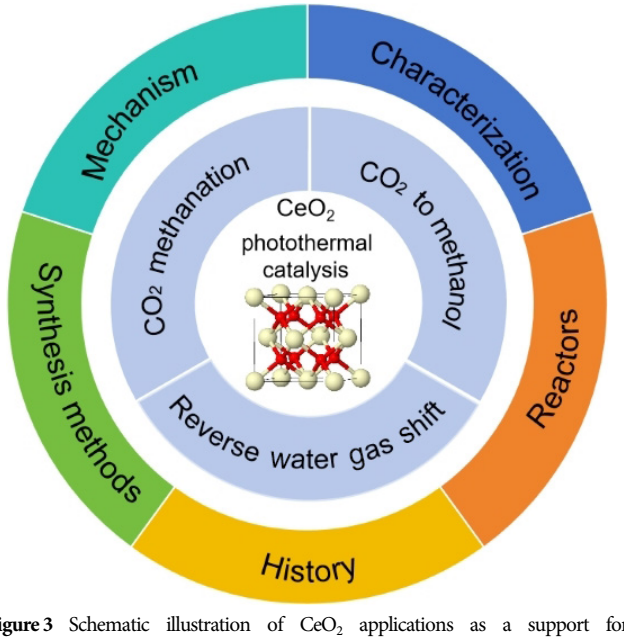

Figure 3 Schematic illustration of CeO_2 applications as a support for photothermal CO_2 hydrogenation reactions.

2 The history of photothermal catalysis

As early as 1911, Eibner observed that illuminating ZnO resulted in the bleaching of Prussian blue pigment, marking the emergence of a novel form of heterogeneous catalysis driven by photon energy-photocatalysis [76]. Subsequently, in 1972, Fujishima and Honda demonstrated that UV light irradiating a cell comprising a TiO_2 photoanode and a Pt counter electrode could generate hydrogen from water [77]. These groundbreaking studies paved the way for extensive research in thermal and photocatalysis, facilitating the production of value-added chemicals. The timeline of ceria-based materials in photothermal catalysis is summarized in Fig. 4. In 1991, J. Melsheimer and others proposed the photothermal photocatalysis concept to increase the reaction temperature and enhance catalytic efficiency during the investigation of Ru/titania catalyzed carbon dioxide methanation [78]. The concept of photo-assisted thermocatalysis was introduced by V. N. Parmon in 1997, in the paper entitled "Photocatalysis as a phenomenon: Aspects of terminology" [79]. Linic and his colleagues introduced the innovative concept of plasmonic catalysis in 2011, by investigating catalytic reactions on silver plasmonic nanostructures under high-temperature illumination [80]. Plasmonic catalysis hinges on the localized surface plasmon resonance (LSPR) effect, propelled by hot charge carriers and thermal energy [81]. However, accurately quantifying their contributions remains a challenge.

Photothermal catalysis using CeO_2-based materials originated two decades ago. Alessandro Trovarelli published a review in 1996, comprehensively describing the catalytic properties of CeO_2 and its potential applications in various catalytic processes [82]. It was the first mention of the photothermal catalysis of CeO_2-containing materials. About a decade ago, there was a surge in the field of photothermal catalysis involving CeO_2-supported metal (M/CeO_2) catalysts. Various M/CeO_2 demonstrated excellent catalytic performance in photothermal catalytic reactions, such as Pd/CeO_2

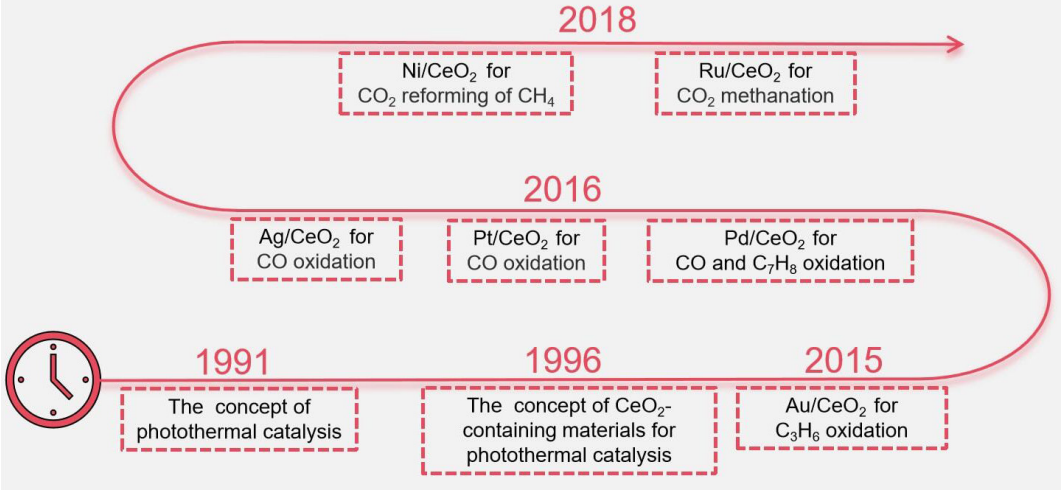

Figure 4 Historical timeline of CeO_2-based materials in photothermal catalysis: 1991, the concept of photothermal catalysis from Ref. [78]; 1996, the concept of CeO_2-containing materials for photothermal catalysis from Ref. [82]; 2015, Au/CeO_2 from Ref. [83]; 2016, Pd/CeO_2 from Ref. [84], Pt/CeO_2 from Ref. [85], Ag/CeO_2 from Ref. [86]; 2018, Ni/CeO_2 from Ref. [87], Ru/CeO_2 from Ref. [88].

[83], Pt/CeO_2 [84], Ag/CeO_2 [85], Au/CeO_2 [86], Ni/CeO_2 [87], Ru/CeO_2 [88] and others. The improved catalytic performance was attributed to the interplay between CeO_2 and metal carrier, instigating various structural modifications such as electronic interactions, active interface site formation and geometric alterations of metal sites, all of which profoundly impact catalytic performance [89]. According to previous reports, the interfacial sites between CeO_2 support and metal sites play an important role in photothermal reactions, the mechanisms involved in these interactions warrant further investigation. Oxygen vacancies in CeO_2 enhance the activity and stability of supported metal nanoparticles (NP). Additionally, Ce^{3+} species, acting as a Lewis base, facilitate the adsorption and conversion of CO_2. For instance, they effectively promote the disproportionation of CO_2 and stabilize CO-containing intermediates. However, the detailed roles of CeO_2-based materials in specific reactions are typically very complex and require thorough investigation to advance the development of novel catalysts.

Recently, a rapid and exciting development has been observed in photothermal catalysis, with a focus on catalyst design to enhance the catalytic performance [90–92]. Photothermal catalysis, as a synergistic integration of thermal and photocatalysis, exhibits superior catalytic performance. This method offers several advantages, including enhanced activity, selectivity and stability, along with mild reaction conditions and reduced costs. It has been widely applied in various chemical processes, demonstrating its effectiveness and versatility [93–95].

3 Synthesis methods for CeO_2-supported catalysts

CeO_2-supported catalysts, particularly those supporting atomic dispersed metals such as single-atom catalysts and highly dispersed nanocluster catalysts, have garnered considerable attention in heterogeneous catalysis owing to their outstanding catalytic performance [58, 99, 100].

Atomic dispersed metal catalysts maximize metal atom utilization, enhancing efficiency and reducing costs [101–125]. Common synthesis methods for CeO_2 include sol–gel, hydrothermal, precipitation and calcination methods, as shown in Fig. 5, each with distinct advantages and limitations affecting particle size, surface area and crystallinity [96, 98].

Advancements in the synthesis and stabilization of CeO_2-supported atomically dispersed metal catalysts have opened new avenues for enhancing the catalytic performance of various processes. Achieving and maintaining atomic dispersion allows the maximum utilization of metal atoms, thus improving the catalytic efficiency and reducing costs [126–129]. This makes these catalysts indispensable in industries where high efficiency and durability are critical, such as automotive catalytic converters, fuel cells and environmental remediation [130–132].

CeO_2 is typically used as a support to load transition or noble metals [135–139]. Achieving atomic dispersion of active metal species on CeO_2 involves careful consideration of the synthetic atmosphere, support material properties and deposition techniques [133, 140–142] (Fig. 6). In contrast, calcination in the air often creates a saturated O-coordinated environment around metal atoms, diminishing catalytic activity due to inadequate activation of reactants [143, 144]. Conversely, H_2 reduction leads to the aggregation of noble-metal single atoms into nanoclusters [141, 143, 144].

Strong interactions between metal atoms and support surfaces are essential for enhanced stability of the catalyst [145]. Modifications like doping or creating defect sites on support materials can further improve dispersion. Doping CeO_2 with Zr or La elements can create oxygen vacancies and alter the electronic properties, stabilizing dispersed metal atoms on the support by acting as traps and preventing aggregation, thereby enhancing catalytic performance [146–148]. Creating defect sites through thermal treatment or plasma exposure also provides additional anchoring points for metal atoms. Deposition methods such as atomic layer deposition (ALD) and photo deposition allow precise control over the placement of metal atoms, ensuring uniform coverage and high catalytic activity [149, 150].

Furthermore, stabilization techniques such as encapsulation within the support material and ligand protection prevent metal atom aggregation, maintaining their dispersion and subsequent catalytic efficiency (Fig. 5(b)) [151]. Encapsulation traps metal atoms within the pores or channels of the support material, protecting them from sintering at high temperatures and ensuring

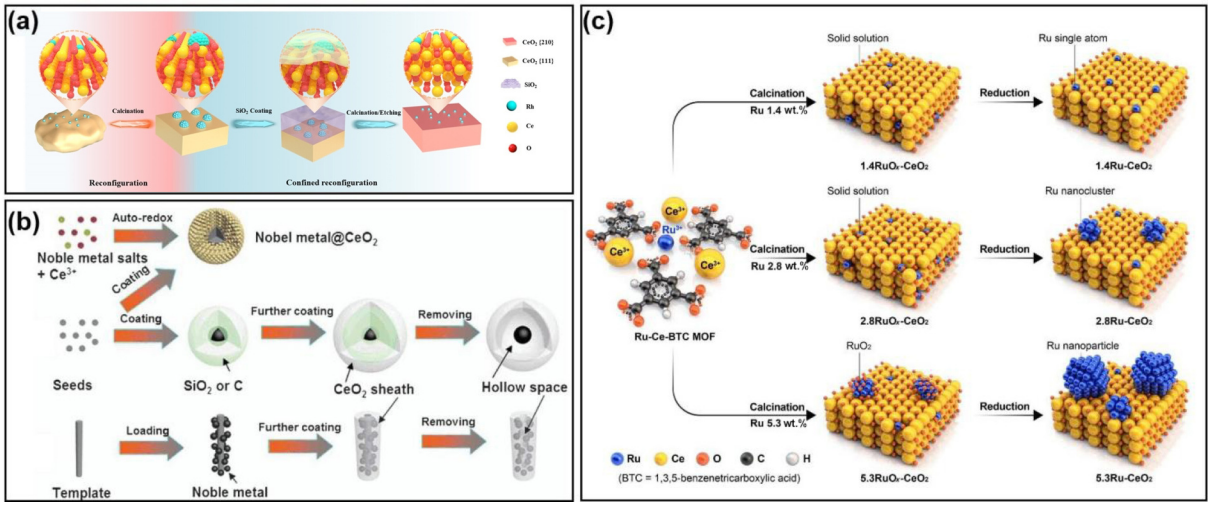

Figure 5 (a) Schematic illustration of "wrap-bake-peel" synthetic strategy. Reproduced with permission from Ref. [96], © Wiley-VCH GmbH 2023. (b) Schematic illustration showing the encapsulation of CeO_2 through various approaches. Reproduced with permission from Ref. [97], © Song, S. et al. 2015. (c) Synthesis of Ru-CeO_2 catalysts. Ru-Ce-BTC (BTC: 1,3,5-benzenetricarboxylic acid), RuO_x-CeO_2 and Ru-CeO_2 represent the raw, calcined and reduced forms, respectively. Reproduced with permission from Ref. [98], © Sivan, S. E. et al. 2022.

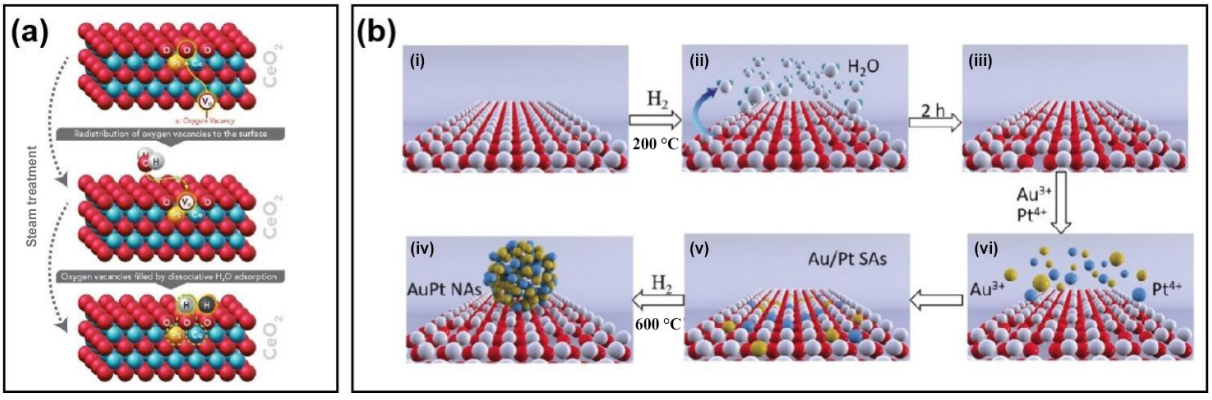

Figure 6 (a) Steam-treatment effects on atomically dispersed Pt/CeO_2 catalyst. Reproduced with permission from Ref. [133], © Nie, L. et al. 2017. (b) Schematic illustration of the catalysts prepared by the solid solvent method. Reproduced with permission from Ref. [134], © Wiley-VCH Verlag GmbH & Co. KGaA, Weinheim 2020. NA refers nanoalloys and SA refers single-atom.

high stability during catalytic reactions [152, 153]. Ligand protection employs organic ligands to stabilize metal atoms during synthesis, preventing their aggregation and enhancing dispersion. These ligands can be removed by activation, leaving behind highly dispersed metal atoms. These advancements in synthesis and stabilization are pushing the boundaries of catalyst performance, promising even greater benefits in the future.

4 Reactors for photothermal catalytic reaction

The design and construction of appropriate photothermal reactors are crucial to achieving satisfactory catalytic performance [154, 155]. So far, various photothermal reactors have been constructed and used to match the optimal reaction conditions for the target catalyst [156, 157]. This part will categorize photothermal reactors into two main branches: reactor types and operation mode, as shown in Fig. 7(a). Fixed-bed and structured reactors will be comprehensively discussed based on their applications in photothermal CO_2 hydrogenation to carbon monoxide (CO), methane (CH_4), methanol (CH_3OH) and olefins [158]. These reactors operate either flow-through or in closed mode, with differences in product analysis methods [159, 160].

Flow-through reactors are characterized by continuously passing the reactant gases over the catalyst, allowing steady-state operation and suitability for continuous industrial processes [164]. These reactors are designed to handle a constant gas flow, which is advantageous for maintaining uniform reaction conditions and integrating with other process units. Conversely, batch reactors operate in a closed environment where a fixed number of reactants are charged and the reaction occurs cyclically (Fig. 7(b)) [165]. Reactions are carried out under controlled conditions (temperature and pressure) in this mode, which may be challenging in a flow-through system. Batch reactors, due to their closed operation, also facilitate the investigation of reaction kinetics and mechanisms, allowing precise monitoring of reactant consumption and product formation [166]. In summary, flow-through reactors are preferred for continuous operations and scalability, while batch reactors are suitable for detailed catalytic reactions and applications requiring precise control over reaction conditions. Flow-through reactors can be further divided into fixed-bed and structured reactors. The choice of reactor type is crucial in the efficiency and effectiveness of the photothermal conversion process, with each design offering unique benefits. Structured photothermal reactors, also known as monolithic reactors, are efficient for CO_2 hydrogenation (Fig. 7(d))

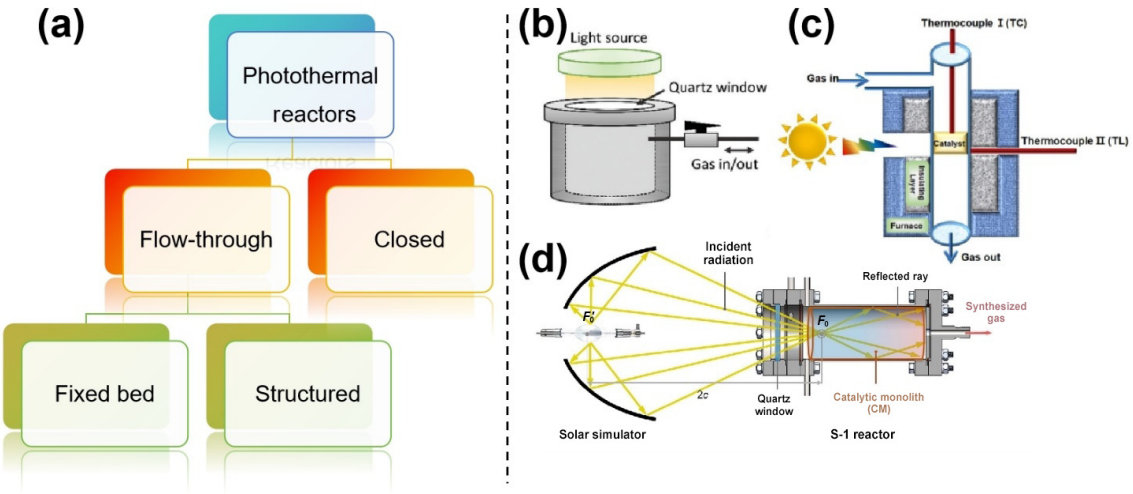

Figure 7 (a) Classification of photothermal reactors. (b) Photothermal closed reactor. Reproduced with permission from Ref. [161], © The Royal Society of Chemistry 2022. (c) Fixed bed photothermal reactors. Reproduced with permission from Ref. [162], © Elsevier B.V. 2022. (d) Structured photothermal reactors. Reproduced with permission from Ref. [163], © Elsevier Ltd. 2018.

[167]. These reactors contain numerous channels, resulting in a higher surface area (100 times) than other support systems [168]. The channel walls are coated with catalysts to enhance contact between reactants and catalysts, facilitating efficient light harvesting as well [169].

Fixed-bed reactors are widely utilized in the photothermal transformation of CO_2 into valuable products due to their high catalytic efficiency, scalability and the ability to maintain a stable reaction environment (Fig. 7(c)) [170, 171]. In this setup, the catalyst is evenly distributed at the bottom of the reactor or supported by materials like quartz [172] or glass [173] fiber filters. This arrangement not only safeguards the catalyst from degradation caused by particle wear but also ensures optimal light exposure. The fixed-bed design also facilitates unhindered light penetration, ensuring that the active surface of the catalyst is fully accessible to photons, which is essential for enhanced photocatalytic activity. This feature is particularly beneficial to maximizing the interaction between the catalyst and light, improving the reaction rates and overall process efficiency. By leveraging the effective light utilization capacity of fixed-bed reactors and their protective environment for the catalyst, these reactors are expected to an optimal choice for photothermal CO_2 conversion to valuable hydrocarbon fuels [174].

5 Characterization methods for photothermal reaction

Characterizing photothermal catalysts is essential for comprehending their catalytic mechanisms and designing efficient catalysts. Many characterization techniques used in traditional thermal and photocatalysis are also applicable to photothermal catalysis [175]. However, the photothermal effect arises from both photochemical and thermochemical contributions. These two mechanisms coexist simultaneously in photothermal reactions; thus, understanding the in-depth reaction mechanism is challenging. Therefore, we summarize specific characterization methods for photothermal catalysis, which may help us gain a deeper understanding of photothermal catalysis.

To investigate the photothermal catalytic mechanism, characterizing the light absorption and photothermal conversion ability is crucial. Qin et al. employed *in situ* ultrafast infrared (IR) spectroscopy to detect short-lived transient species by various catalysts and differentiate their photocatalytic behaviors under photon excitation. This approach delineated the distinctions between photocatalysis and photothermal catalysis [176]. Additionally, *in situ* ultrafast visible (Vis) pump/IR probe spectroscopy was utilized to monitor photon-induced electron excitation and transfer. Jiang et al. used electromagnetic simulations to demonstrate that the local electromagnetic field at the Au/CeO_2 interface was intensified more than 100-fold under 615 nm light irradiation [177]. The hot electrons electrons are within the gold nanoparticles, which are then injected into the CeO_2 catalyst.

Another approach to understanding photothermal reactions involves direct temperature measurement at surface active sites. Thermoreflectance and optical interferometry techniques utilize light reflection for thermal measurements. Thermoreflectance relies on the relationship between the material's refractive index and temperature, generating temperature profiles at micrometer/submicrometer scale with high thermal and temporal resolutions, typically around 0.01 K and 0.1 μs, respectively [180]. Due to its extensive use in microelectronics for monitoring electrical self-heating, Wang et al. employed various thermoreflectance techniques to evaluate the thermal enhancement in Au/Al_2O_3 plasmonic structures, achieving remarkable spatial and temporal resolutions of approximately 100 nm and several nanoseconds, respectively [181]. Sabastine et al. introduced near-field scanning thermoreflectance imaging (NeSTRI) a novel non-contact technique that combines a modulated pump laser with a continuous-wave probe laser and near-field optical microscopy (SNOM) to map the thermal properties of thin films at nanoscale. They employed multilayer graphene films as a case study, demonstrating the capability for high-resolution imaging and quantification for thermal conductivity and specific heat (Fig. 8(a)) [178]. Besides, IR thermography is also suitable for thermal measurements. The estimation of a body's temperature profile based on the Planck blackbody emission principle involves analyzing its emitted energy [182]. Thermal mapping through IR cameras combined with bulk thermocouple measurements facilitates the determination of local and global temperatures. Liu et al. used an IR camera to measure the catalyst temperature (TC) and local temperature (TL) of a Pd/C catalyst [162].

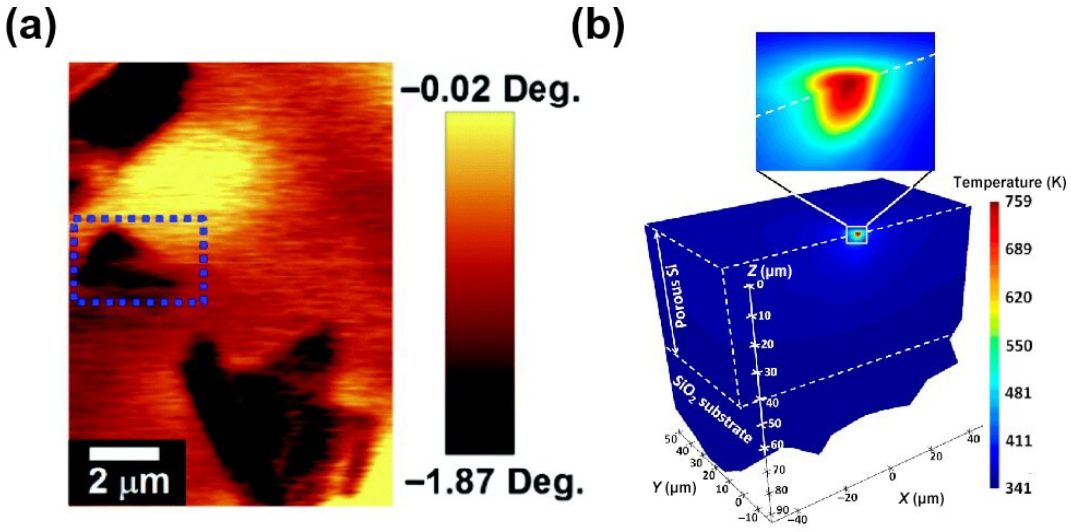

Figure 8 (a) NeSTRI phase images at 75 Hz pump beam modulation frequency in non-contact from the test sample. Reproduced with permission from Ref. [178], © The Royal Society of Chemistry 2017. (b) In-depth *T* distribution of porous Si NP films deposited on 1 mm thick SiO_2 glass substrate. Reproduced with permission from Ref. [179], © Kurbanova, B. A. et al. 2021.

The significant temperature difference confirmed the applicability of this photothermal material, achieving high temperatures at specific positions while maintaining lower temperatures in the surrounding environment. Bayan et al. investigated the photothermal effects and heat conduction in nanogranular silicon films, revealing a cubic-to-hexagonal phase transition induced by laser heating and demonstrating the control over thermal conductivity of these films by adjusting the film thickness, nanoparticle size and porosity (Fig. 8(b)) [179].

In recent years, an increasing number of emerging characterization methods have been applied to the field of photothermal catalysis. These methods can monitor changes in properties and investigate catalytic mechanisms. A correlation has been established between characterization results and catalyst efficacy, revealing new phenomena that highlight the precision and applicability of these techniques [175].

6 Photothermal catalytic transformation of CO_2

The solar-powered reduction of CO_2, known as "artificial photosynthesis", has the potential to decrease CO_2 emissions and mitigate global warming [183–185]. The CO_2 reduction products can be categorized into C1 compounds (CO, CH_4, CH_3OH) and C_{2+} compounds (multi-carbon alkanes and olefins) [186, 187]. C1 compounds are essential raw materials for manufacturing plastics, fuels and fertilizers, attracting significant global interest. These products are manufactured through reverse water gas shift reaction (RWGS), CO_2 methanation, methanol synthesis and other reactions. In the past decade, there has been exponential growth in photothermal catalysis to accelerate these reactions. The optimal temperatures and performance metrics of catalysts used for photothermal CO_2 conversion are summarized in Fig. 9.

6.1 Reverse water gas shift reaction

The RWGS is widely recognized as the primary reaction in CO_2 hydrogenation to produce CO and H_2O, serving as the initial step in CO_2 conversion processes, such as methanol synthesis and hydroformylation using CO_2 [188]. CeO_2, as a metal oxide catalyst, demonstrates promising catalytic performance in the RWGS due to its unique redox properties in heterogeneous catalysis, distinguishing it from other conventional oxides such as Al_2O_3 and SiO_2 [189–191]. Two reaction pathways, the redox pathway and the

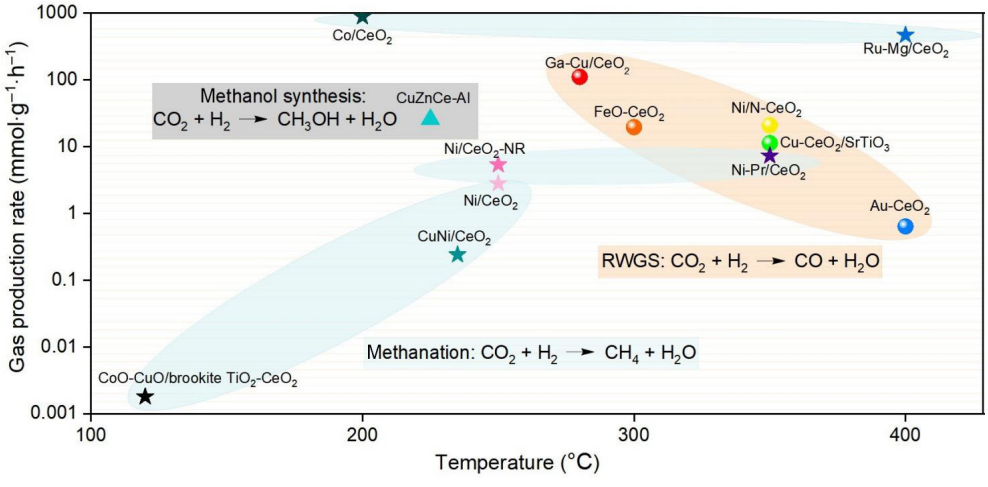

Figure 9 Summary chart of catalytic performance of CeO_2-based catalysts.

associative pathway, can coexist over this type of catalysis [9]. CeO_2 in M/CeO_2 catalysts plays an essential role by mutual tuning effects with metals. The catalytic performance of representative CeO_2-based catalysts is compared in Table 1.

Light-responsive supported metals (e.g., Cu, Fe and Au) are promising catalysts for photothermal RWGS [189, 198]. Ye et al. reported a Ga-Cu/CeO_2 catalyst that achieved a CO production rate of 111.2 $mmol \cdot g^{-1} \cdot h^{-1}$ with nearly 100% selectivity under full solar spectrum irradiation (Fig. 10(a)) [193]. Combining photothermal heating and light irradiation significantly increased the CO production efficiency. Incorporating Ga promoted the production of formate species, which are key intermediates in CO_2 hydrogenation. Moreover, light irradiation facilitated the conversion of the formate species to carbonyl compounds, further boosting CO production (Fig. 10(b)). Lu et al. synthesized an Au/CeO_2 catalyst and the photothermal RWGS achieved a high conversion rate and CO selectivity [195]. The photothermal reaction rate was significantly 10 times higher than that of thermal-only conditions (Fig. 10(c)). The unique role of light promoted the hydrogen-splitting step. Under photothermal conditions, hydrogen molecules were efficiently dissociated, leading to the formation of Au-H species (Fig. 10(d)).

The LSPR and intraband/interband transitions are essential to shaping the optical properties of nanometals [74]. Chemical reactions can be initiated when nanometals are exposed to light with sufficient energy, resulting in the generation of energetic hot carriers and localized thermal energy. Zhang et al. synthesized the Cu/CeO_2 catalyst, demonstrating excellent RWGS catalytic activity and CO selectivity, with significantly increased CO production (30%) at 250 °C under light irradiation (Fig. 10(e)) [196]. The LSPR generated by Cu nanoparticles stimulates the hot electrons transfer under visible light irradiation, which attacks bidentate formates and linear CO intermediates, accelerating their decomposition and desorption to CO while inhibiting further CO reduction (Fig. 10(f)). Zhu et al. synthesized a three-phase Cu-CeO_2-$SrTiO_{3-\delta}$ catalyst [197]. This catalyst, featuring a unique multiphase heterojunction that demonstrated excellent performance, achieving a CO yield of 11.32 $mmol \cdot g^{-1} \cdot h^{-1}$ with a high CO selectivity of 99.95%, 9 times greater than that of pure $SrTiO_3$ (Fig. 10(g)). The enhanced activity is primarily attributed to the synergistic effects of incorporating three phases: Cu nanoparticles, CeO_2 and $SrTiO_{3-\delta}$ interfaces. Similar to Cu/CeO_2, the LSPR effect of Cu nanoparticles significantly promoted the catalytic performance of RWGS (Fig. 10(h)).

Zhao et al. synthesized FeO-CeO_2 nanocomposite catalysts that demonstrated remarkable photothermal CO_2 reduction efficiency [192]. Notably, the FeCe-300 catalyst, with an optimal Fe to Ce molar ratio of 2:1, achieved a high CO_2 conversion rate (43.63%) and an outstanding CO selectivity (99.87%) under Xe lamp irradiation (Fig. 11(a)). The enhanced performance was attributed to FeO and CeO_2 nanoparticles, which promoted the photothermal RWGS reaction. Characterization results provided insights into the

Table 1 Summary of catalytic performance of CeO_2-based catalysts in the RWGS

Catalyst	Catalyst amount (mg)	Product yield ($mmol \cdot g^{-1} \cdot h^{-1}$)	Selectivity (%)	Temperature (°C)	References
FeO-CeO_2	50	19.61	99.87	300	[192]
Ga-Cu/CeO_2	10	111.2	100	280	[193]
Ni/N-CeO_2	50	20.9	100	350	[194]
Au/CeO_2	50	0.64	100	400	[195]
Cu/CeO_2	240	—	100	250	[196]
Cu-CeO_2/$SrTiO_3$	150	11.32	99.95	350	[197]

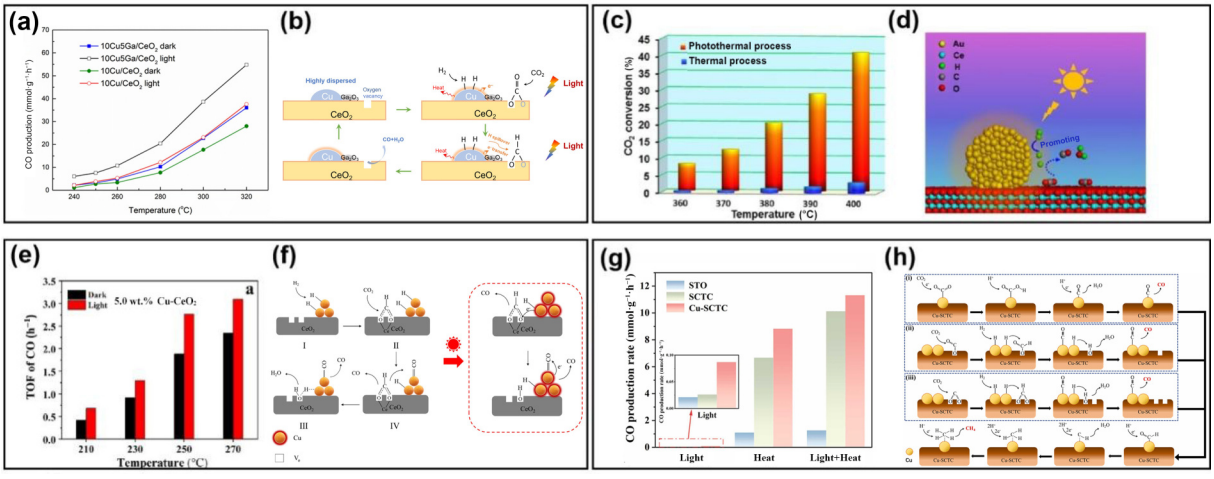

Figure 10 (a) CO production using 10Cu/CeO_2 and 10Cu_5Ga/CeO_2 catalysts as a function of temperature under dark and light conditions. (b) Proposed reaction mechanism for photothermal RWGS over Ga-Cu/CeO_2. Reproduced with permission from Ref. [193], © Elsevier B.V. 2021. (c) CO_2 conversion by the Au/CeO_2 in the photothermal or thermal process. (d) Schematic diagram of enhanced CO_2 conversion in photothermal process using Au/CeO_2. Reproduced with permission from Ref. [195], © Elsevier B.V. 2019. (e) Catalytic performance of 5.0 wt.% Cu/CeO_2. (f) Proposed reaction mechanism for photothermal RWGS using Cu/CeO_2. Reproduced with permission from Ref. [196], © Elsevier Ltd. 2022. (g) CO production rates of $SrTiO_3$ (STO), desired crystalline Cu^{2+}-doped, CeO_2-loaded $SrTiO_{3-\delta}$ perovskite oxide (denoted as SCTC) and Cu-SCTC catalysts under dark, light and photothermal conditions. (h) Possible reaction pathways for the CO_2 reduction to CO using Cu-CeO_2-$SrTiO_{3-\delta}$. Reproduced with permission from Ref. [197], © Zhu, Z. H. et al. 2024.

structure and key reaction intermediates, including formate, bicarbonate and methanol (Fig. 11(b)). The experimental findings highlighted the potential of FeO-CeO_2 nanocomposites for highly selective and stable solar-driven CO_2 conversion to CO, offering significant economic and environmental benefits. Jia et al. synthesized Ni nanoparticle-loaded N-doped CeO_2 (Ni/N-CeO_2) composite through a three-step method, which demonstrated exceptional photothermal CO_2 reduction performance [194]. The optimal Ni/$N_{5.0}$-CeO_2 achieved a CO yield of 20.9 mmol·g^{-1}·h^{-1} and nearly 100% CO selectivity (Fig. 11(c)). This superior catalytic activity was due to the strong light absorption facilitated by Ni nanoparticles and an enhanced CO_2 adsorption/activation due to additional oxygen vacancies from N-doping, promoting the CO_2 reduction to CO while suppressing the methanation process (Fig. 11(d)).

6.2 CO_2 methanation

CO_2 methanation, also known as the Sabatier reaction, is another common reaction in CO_2 hydrogenation [199, 200]. This reaction has been extensively explored to convert electrical energy into fuel, especially in regions lacking fossil energy but with abundant, low-cost electrical power available for H_2 production [201]. Transition metal sites are essential in CO_2 methanation catalysts since the reaction consumes more hydrogen atoms compared to the RWGS [202].

Table 2 indicates that most of the studies have focused on Ni, Ru and other group VIII metal catalysts for CO_2 methanation. Various transitional or noble metals have been intensively applied for CO_2 methanation [211–215]. Golovanova et al. synthesized a Ni/CeO_2 catalyst with a high CO_2 conversion efficiency (80%) and an impressive CH_4 selectivity (95%) [209]. Notably, the reaction rate under sunlight irradiation was 2.4 times higher than in the dark (Fig. 12(a)). Two key factors contributed to this enhancement: the LSPR effect of Ni nanoparticles under light generates heat, increasing the catalyst surface temperature and boosting reaction efficiency and CeO_2 support possesses photocatalytic activity, with light-excited carriers promoting the formic acid species

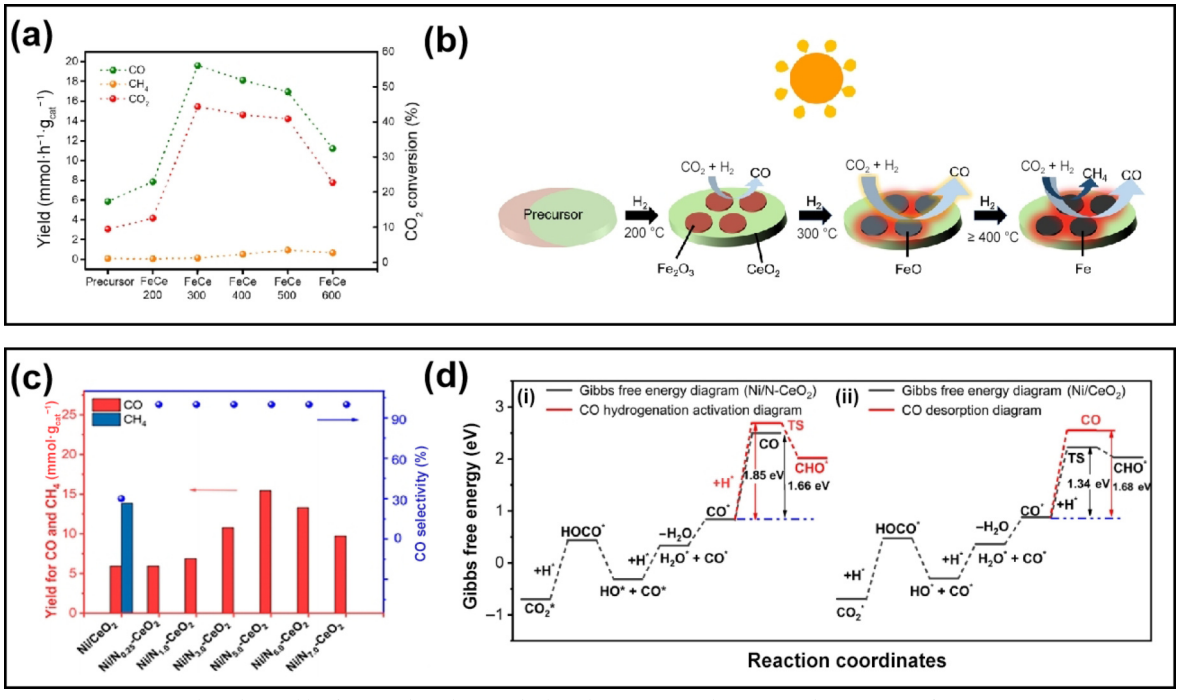

Figure 11 (a) CO_2 conversion and product yields of CH_4 and CO by FeCe hydroxide precursor and FeCe-*x* catalysts (a series of FeO-CeO_2 nanocomposite catalysts were successfully prepared by H_2 reduction of $Fe(OH)_3$-$Ce(OH)_3$ precursors at temperatures (*x*) ranging from 200 to 600 °C (the obtained catalysts are denoted as FeCe-*x*)). (b) Fabrication of FeCe-*x* catalysts by reduction of $Fe(OH)_3$-$Ce(OH)_3$ precursors at 200–600 °C. Reproduced with permission from Ref. [192], © Zhao, J. Q. 2020. (c) Photothermal CO_2 reductions by Ni/CeO_2 and Ni/N_x-CeO_2. (d) Gibbs free energy diagrams of Ni/N-CeO_2 for CO_2 reduction to CO and CHO*. Reproduced with permission from Ref. [194], © American Chemical Society 2021.

Table 2 Summary of catalytic performance of CeO_2-based catalysts in CO_2 methanation

Catalyst	Catalyst amount (mg)	Product yield (mmol·g^{-1}·h^{-1})	Selectivity (%)	Temperature (°C)	References
Ni/CeO_2	75	9.12	99.3	250	[203]
Co/CeO_2	100	885.27	97.34	200	[204]
CoO-CuO/TiO_2-CeO_2	200	0.0018	—	120	[205]
CuNi/CeO_2	300	0.24	—	235	[206]
Ni/CeO_2-NR	50	5.36	100	250	[207]
Ni/Pr-CeO_2	200	7.3	100	350	[208]
Ni/CeO_2	—	2.8	95	250	[209]
Ru/Mg-CeO_2	30	469	93.1	400	[210]

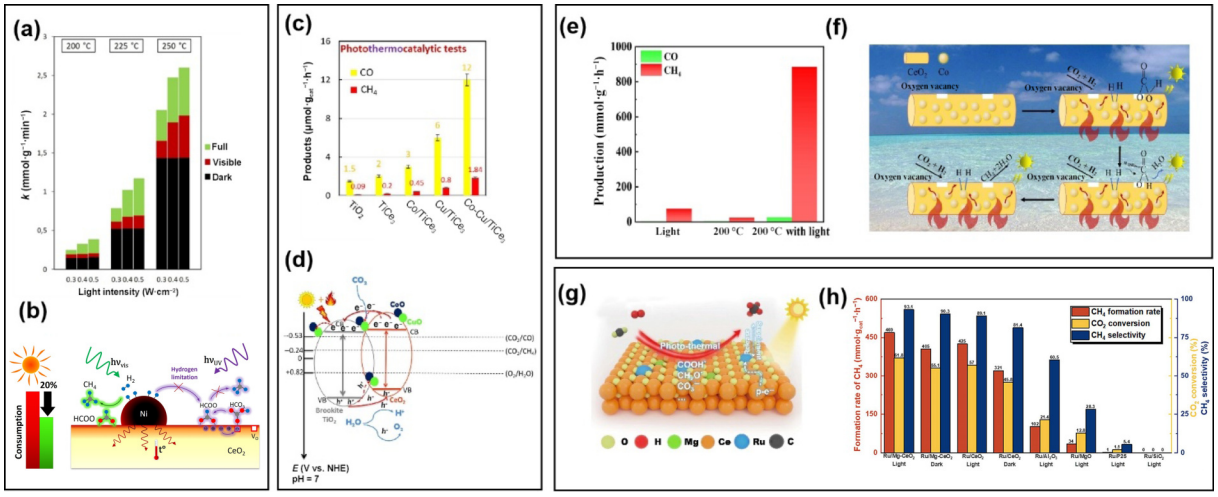

Figure 12 (a) The catalytic activity of Ni/CeO_2 catalyst under visible light and solar illumination of 3 to 5 suns at three different starting temperatures. (b) Proposed mechanism of CO_2 methanation under solar irradiation. Reproduced with permission from Ref. [209], © Golovanova, V. et al. 2021. (c) Photothermocatalytic tests at T = 120 °C on $TiCe_3$-based samples. (d) Proposed photothermocatalytic mechanism of Co-Cu/$TiCe_3$ catalyst. Reproduced with permission from Ref. [205], © Elsevier B.V. 2021. (e) CO_2 reduction activity of CC-1:1 comparison test under light and at 200 °C. (f) Photothermal catalytic CO_2 reduction mechanism for Co/CeO_2. Reproduced with permission from Ref. [204], © Elsevier B.V. 2023. (g) CH_4 formation rate, CO_2 conversion and CH_4 selectivity for different catalysts. (h) Proposed mechanism of CO_2 methanation by Ru/Mg-CeO_2. Reproduced with permission from Ref. [210], © Elsevier Inc. 2024.

formation, altering the reaction pathway and enhancing methane selectivity (Fig. 12(b)). Fiorenza et al. investigated the solar photothermocatalytic conversion of CO_2 using CoO-CuO/brookite TiO_2-CeO_2 catalysts [205]. The bimetallic oxide-based catalyst demonstrated superior photocatalytic performance, achieving higher CO and CH_4 formation rates than pure brookite (Fig. 12(c)). Furthermore, the photothermal approach with the CoO-CuO/TiO_2-CeO_2 catalyst substantially enhanced CO_2 conversion, highlighting the strong interaction between CO_2 and catalyst surface sites (Fig. 12(d)).

Pan et al. developed a highly efficient Co/CeO_2 catalyst, which demonstrated a notable CH_4 yield of 885.27 mmol·g^{-1}·h^{-1} and a CO yield of 24.5 mmol·g^{-1}·h^{-1} (Fig. 12(e)) [204]. Examining the reaction mechanism under photothermal catalysis revealed that the efficient CH_4 and H_2O production from formate hydrogenation was facilitated by hot carriers (Fig. 12(f)). Additionally, Zhang et al. developed a Ru/Mg-CeO_2 single-atom catalyst for efficient photothermal CO_2 methanation, achieving a high CH_4 formation rate of 469 mmol g^{-1} h^{-1} with excellent stability at 400 °C (Fig. 12(g)) [210]. The catalyst achieved superior performance due to the synergistic effects of single-atom Ru, Ru–O–Ce structure and Mg doping (Fig. 12(h)).

Yue et al. reported that the CuNi/CeO_2 catalyst demonstrated distinct product selectivity in photothermal CO_2 reduction reactions under dark and visible light conditions [206]. Visible light promoted further hydrogenation to CH_4, revealing that the electrons transfer between Cu and Ni altered the thermal reduction and enhanced CO_2 trapping via increased surface hydroxyl and oxygen vacancies (Fig. 13(a)). This study presented insights into the non-thermal effects of photothermal catalysis (Fig. 13(b)). Bian et al. investigated the morphology dependence of Ni/CeO_2 catalysts,

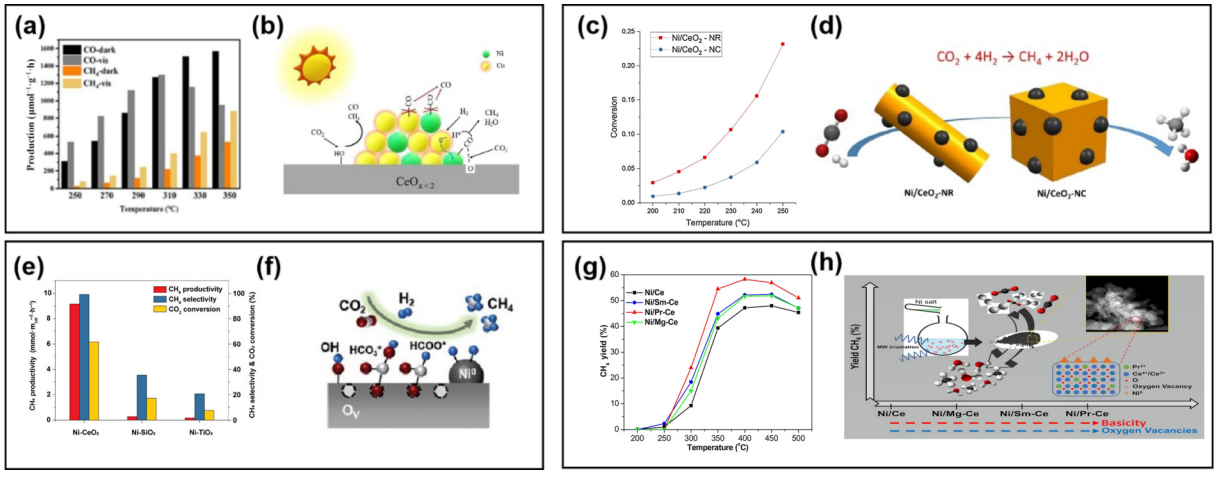

Figure 13 (a) The catalytic activity of Cu_5Ni_3/CeO_2 at different temperatures. (b) Schematic diagram of the photothermal catalytic mechanism of Cu_5Ni_3/CeO_2. Reproduced with permission from Ref. [206], © Elsevier B.V. 2023. (c) Catalytic conversion test of Ni/CeO_2. (d) Proposed mechanism of CO_2 methanation by Ni/CeO_2. Reproduced with permission from Ref. [207], © Elsevier B.V. 2018. (e) Comparison of photothermal methanation performance of Ni/CeO_2, Ni/TiO_2 and Ni/SO_2. (f) Schematic illustration of photothermal CO_2 methanation reaction mechanism using Ni/CeO_2 catalysts. Reproduced with permission from Ref. [203], © Wiley-VCH GmbH 2023. (g) Catalytic performance of Ni/Ce, Ni/Sm-Ce, Ni/Pr-Ce and Ni/Mg-Ce as a function of reaction temperature. (h) Proposed CO_2 methanation mechanism by Ni/CeO_2. Reproduced with permission from Ref. [208], © Elsevier B.V. 2020.

suggesting that Ni/CeO_2 nanorods (NR) exhibited higher methanation activity and selectivity compared to nanocubes (NC) at low temperatures (Fig. 13(c)) [207]. Characterization techniques indicated that Ni/CeO_2-NR exhibited a higher proportion of Ce^{3+}. The presence of more oxygen vacancies served as active sites for formate production in the methanation mechanism (Fig. 13(d)). This research provides a novel strategy to prepare efficient catalysts and conduct fundamental kinetic and mechanistic studies in heterogeneous catalysis.

Zhang et al. developed a hydrothermal growth strategy that selectively targets CO_2 to synthesize CeO_2 octahedral nanocrystals, exhibiting strong physicochemical interactions with CO_2 molecules, significantly enhancing photothermal CO_2 hydrogenation to methane [203]. The Ni-loaded CeO_2 catalyst demonstrated superior performance with a CH_4 production yield of over 9 $mmol \cdot h^{-1} \cdot m_{cat}^{-2}$ and a selectivity higher than 99%, possibly due to the abundant oxygen vacancies and hydroxyl species on the CeO_2 surface that created numerous active sites and the strong metal-support interaction that enhanced H_2 dissociation and CO_2 hydrogenation (Figs. 13(e) and 13(f)). This approach presented a novel pathway for developing catalysts with targeted properties for specific chemical reactions. Siakavelas et al. comprehensively investigated CO_2 methanation reaction over Ni catalysts supported on CeO_2, Sm_2O_3-CeO_2, Pr_2O_3-CeO_2 and MgO-CeO_2 binary oxides [208].

The catalysts were synthesized by a microwave-assisted sol–gel method and characterized by various techniques. Adding Sm^{3+} or Pr^{3+} to CeO_2 generated oxygen vacancies and restricted nickel agglomeration, thus improving low-temperature hydrogenation and enhancing CO_2 methanation activity.

Particularly, the Ni/Pr-Ce catalyst demonstrated the highest CO_2 conversion and CH_4 yield of 54.5% each, along with 100% selectivity at 350 °C (Fig. 13(g)). The Mg^{2+} addition created strong metal-support interactions, enhancing the catalyst's resistance to sintering and providing a crucial understanding of the role of non-thermal effects in photothermal catalysis (Fig. 13(h)).

6.3 CO_2 conversion to methanol

Compared to CO and CH_4 production, the CO_2 reduction to methanol holds greater economic appeal [216, 217]. Methanol, a pivotal platform chemical, can be further converted to olefins, aromatics and dimethyl ethers through well-established processes [218, 219]. Global methanol production currently stands at 106 million metric tons per year [220]. Methanol-to-olefin conversions represent 31.5% of global methanol consumption, marking a significant growth over the past decade [221]. Another substantial application of methanol is in the transport sector, where it constitutes 27% of methanol consumption [222]. In this sector, methanol is utilized either directly as a fuel or blended with gasoline, providing a cleaner-burning alternative to pure gasoline. Methanol, as a liquid fuel, boasts relative ease of transportation, storage and distribution [223]. Consequently, methanol production from CO_2 reduction has become an increasingly attractive area for researchers worldwide [225, 226]. While a variety of catalysts can catalyze the RWGS reaction, methanol production relies heavily on a select group of transition metal catalysts, such as Cu, Ag, Au and Pd [227, 228]. Among these, Cu-based catalysts are the most extensively used due to their cost-effectiveness for large-scale applications [229]. Numerous oxides have been explored as supports in methanol synthesis, such as ZnO, Al_2O_3, TiO_2, ZrO_2, SiO_2, Cr_2O_3 and CeO_2 [230]. CeO_2-based materials have attracted growing attention in methanol synthesis reactions due to their distinctive catalytic properties. Xie et al. fabricated a ceria-modified Cu/ZnO/Al_2O_3 catalyst (CuZnCe-Al) that significantly enhanced

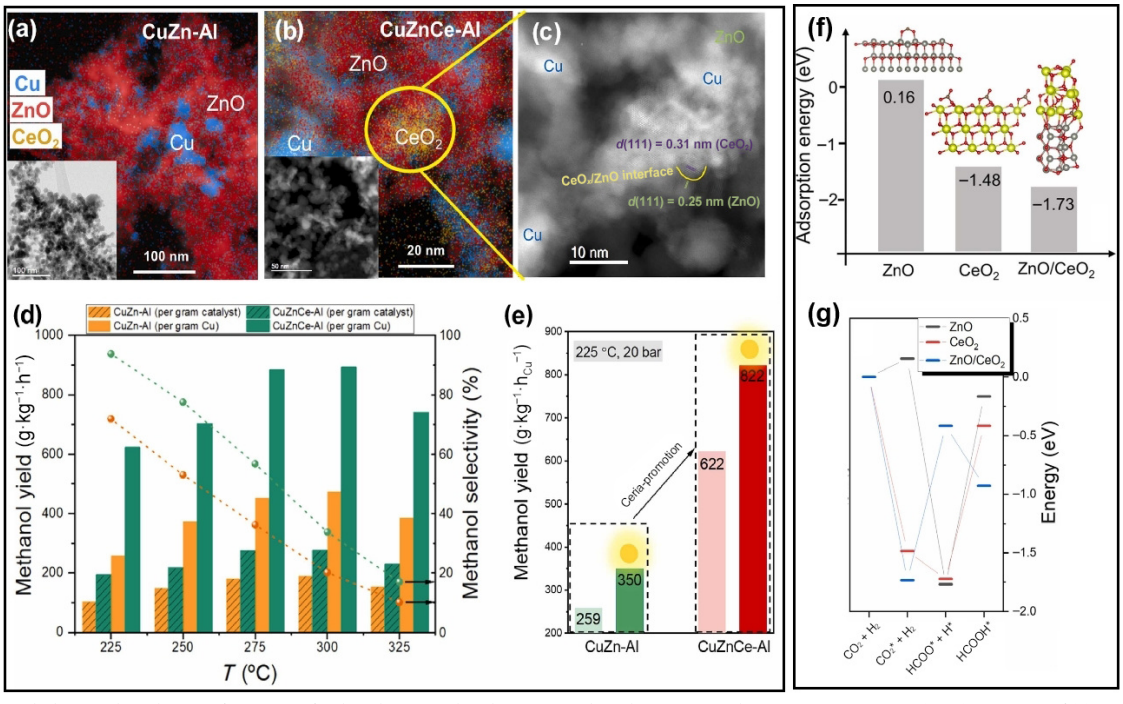

Figure 14 Morphology and catalytic performance of reduced CuZn-Al and CuZnCe-Al catalysts. Energy dispersive spectroscopy (EDS) mapping of (a) CuZn-Al and (b) CuZnCe-Al. The inset shows the corresponding TEM image of each sample. (c) HRTEM image of CuZnCe-Al microstructure. (d) Methanol selectivity and space-time yield under dark conditions when normalized to the mass of the catalyst and the mass of Cu. (e) Catalytic activity at 225 °C under dark and light conditions. (f) Adsorption energies of CO_2 on constructed ZnO, CeO_2 and ZnO/CeO_2 model structures. (g) Energy profiles of elementary steps for formate production and hydrogenation over ZnO, CeO_2 and ZnO/CeO_2 interface. Reproduced with permission from Ref. [224], © Elsevier B.V. 2022.

low-temperature methanol production from CO_2 hydrogenation under light irradiation.

Figures 14(a)–14(c) displays the high-resolution transmission electron microscopy (HRTEM) images and elemental mapping of Cu-ZnO-Al_2O_3 (CuZn-Al) and ceria-modified (CuZnCe-Al) catalysts. Figure 14(d) illustrates the catalytic activity and selectivity of both materials at 21 bar. The catalysts demonstrated a yield of 822 $g{\cdot}kg^{-1}{\cdot}h_{Cu}^{-1}$ and a selectivity of 94% at 225 °C and 20 bar (Fig. 14(e)). The results reveal that an optimal CeO_2 content promotes CO_2 chemisorption and the formate pathway, beneficial for methanol synthesis. The findings underscore the potential of CeO_2-promotion and photo-activation strategies to improve the CO_2 conversion efficiency to methanol, offering a sustainable approach to utilizing CO_2 as a chemical feedstock (Figs. 14(f) and 14(g)).

The robust interaction between metal particles and the CeO_2 support inhibits the metal particles sintering during catalyst preparation [231, 232], creating smaller metal particles and a narrower size distribution than other oxide supports like ZrO_2 and Al_2O_3 [233]. The high metal dispersion can enhance the hydrogen dissociation, thereby increasing the concentration of surface H atoms and facilitating the oxygen vacancies generation through surface reduction. Moreover, the highly dispersed metal particles elevate metal-support interface sites, playing a crucial role in CO_2 activation and methanol production [234].

6.4 Reaction mechanism

So far, two main reaction mechanisms have been proposed in the literature for the photothermal reaction over CeO_2-based materials [9]. One is the redox mechanism, where Ce^{4+}-O-Ce^{4+} species on the surface of CeO_2 are reduced by H_2 to produce H_2O and □ (oxygen vacancy) adjacent to Ce^{3+} species (Ce^{3+}-□-Ce^{3+} species). Ce^{3+}-□-Ce^{3+} species are then reoxidized by CO_2 to yield CO and Ce^{4+}-O-Ce^{4+} species [235, 236]. The other is the associative mechanism, which involves the formation and conversion of intermediates, such as formate or carboxyl groups. In this pathway, CO_2 is adsorbed onto the catalyst surface and reacts with adsorbed hydrogen to form a key intermediate. The efficiency of this pathway relies on surface OH groups, which act as the primary active sites for CO_2 adsorption and activation, due to the absence of adsorbed O^{2-} sites [237, 238].

6.5 Stability

Heterogeneous catalysis often deals with processes of direct industrial relevance. In such cases, the ability to produce large product volumes is crucial, which translates into the need for long catalyst lifetimes-usually months-in order to reduce costs [239]. Catalyst stability, intended as the ability to retain catalytic function over time rather than structural stability, is routinely assessed through time-on-stream or recycling experiments. Figure 15 shows the stability of some photothermal catalysts. However, these tests are occasionally performed with reactions run at full conversion [240]. In these cases, the reactions are limited by the amount of available reagent and a potential activity decrease would not be revealed. Since those conditions do not reflect a kinetically controlled regime, any stability claim remains unsupported. Best practice, in this case, suggests performing experiments at low conversion or away from equilibrium conversion.

7 Conclusion and perspective

Reducing CO_2 emissions has become a critical objective in global ecological environmental protection efforts. Photothermal catalytic CO_2 hydrogenation holds significant promise in curbing atmospheric CO_2 levels and fostering a high-quality carbon cycle due to its inherent efficiency, environmental friendliness and sustainability. The main products of photothermal catalysis are CH_4, CO and CH_3OH, with high yield and selectivity. Of all the

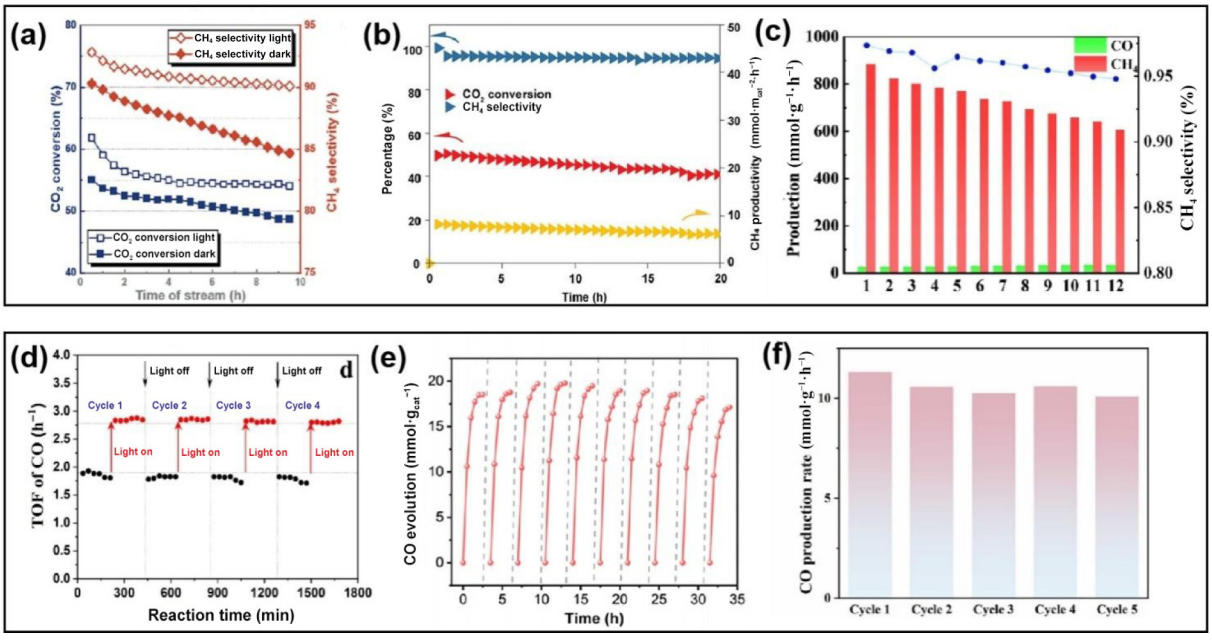

Figure 15 (a) Stability of Ru/Mg-CeO_2 for CO_2 methanation. Reproduced with permission from Ref. [210], © Elsevier Inc. 2024. (b) Stability of Ni/CeO_2-CO_2 in photothermal CO_2 methanation. Reproduced with permission from Ref. [203], © Wiley-VCH GmbH 2023. (c) 12 h stability test at 200 °C for CC-1:1. Reproduced with permission from Ref. [204], © Elsevier B.V. 2023. (d) The stability test of Cu-CeO_2 for RWGS reaction under visible light and dark conditions. Reproduced with permission from Ref. [196], © Elsevier Ltd. 2022. (e) 10 cycles of reaction over Ni/$N_{5.0}$-CeO_2. Reproduced with permission from Ref. [194], © American Chemical Society 2021. (f) Photothermal stability cycling experiments of Cu-SCTC catalysts. Reproduced with permission from Ref. [197], © Zhu, Z. H. et al. 2024.

reported catalysts in RWGS, the Ga-Cu/CeO_2 catalyst synthesized by Ye et al. achieved the best performance, with a CO yield of 111.2 mmol·g^{-1}·h^{-1} [193]. For CO_2 methanation, the Co/CeO_2 catalyst prepared by Pan et al. demonstrated an impressive yield of 885.27 mmol·g^{-1}·h^{-1} [204]. However, very few photothermal cerium-based catalysts have been developed for methanol synthesis. For example, the CuZnCe-Al catalyst reported by Xie et al. achieved a performance of 822 g·kg^{-1}·h_{Cu}^{-1} [224]. The extensive efforts dedicated to utilizing Ce-based photothermal catalysts yielded extremely promising prospects in CO_2 hydrogenation to value-added products. Nevertheless, several aspects of photothermal CO_2 hydrogenation still need attention and warrant future investigation, as detailed below;

(1) Advanced photothermal catalysts development. In current studies, the primary products of photothermal CO_2 reduction are CO and CH_4. At the same time, some studies have reported producing other high-value products such as methanol, ethanol, or C_{2+} hydrocarbons in photothermal CO_2 reduction systems. However, there remains a substantial gap between current progress and meeting the actual demand. Researchers are focusing on developing novel photothermal catalysts with enhanced light absorption and heat management capabilities, including bimetallic nanoparticles and hybrid materials. Furthermore, developing photothermal catalysts that maintain activity over extended periods and resist deactivation is crucial for practical applications. Fine-tuning reaction conditions to control product selectivity remains a key challenge. Advanced materials and reaction engineering are essential to achieve the desired outcomes.

(2) Recognition of photothermal catalytic reaction mechanism. The mechanism of photothermal CO_2 reduction systems under solar energy remains to be fully explored. To advance the study of photothermal catalytic processes, it is crucial to develop *operando* methods rather than *in situ* methods to establish correlations between spectral changes and product formation, enabling direct identification of reaction intermediates and thereby deducing reaction mechanisms. Without this, some spectral changes might only be artifacts rather than reflecting the dynamic changes on the catalyst surface. For instance, *in situ* IR has previously focused primarily on spectral changes of adsorbed species [236, 241]. These changes could merely be the result of side reactions, rather than representing intermediates in the reaction process. Therefore, *operando* characterization methods should be developed to investigate the real reaction intermediates.

(3) Aggregation and dispersion behavior of active metals under photothermal conditions. The interaction between the CeO_2 surface and active metal sites varies with temperature and different reaction atmospheres. It will be necessary in the future to conduct comprehensive studies on the aggregation and dispersion behavior of active metals on CeO_2 surfaces under photo-thermal conditions. Based on the experience in pervious atomic dispersion [99], it is essential to develop *in situ* observation techniques to study the dynamic of active sites under photo, thermal and photo-thermal conditions. This will provide a clear understanding of the influence of light-induced electron–hole pairs on metal dispersion, facilitating the development of high-performance CeO_2-based catalysts.

(4) Integration with carbon capture. Combining photothermal catalysis for CO_2 conversion with carbon capture could transform CO_2 under mild conditions, contributing to establishing a new carbon cycle. Therefore, developing continuously operatable photothermal catalytic systems for CO_2 capture and conversion, along with related high-performance catalysts, is a significant future research area.

Data availability

Not applicable.

Acknowledgements

The work was financially supported by the National Natural Science Foundation of China (Nos. 22172069 and 22106085).

Declaration of competing interest

All the contributing authors report no conflict of interests in this work.

Author contribution statement

Z. R. Z.: Investigation, writing – original draft. X. H.: Writing – review & editing. J. H. Z.: Supervision, writing – review & editing. Y. Y. D.: Writing – review & editing. J. S. Z.: Supervision, funding acquisition, writing – review & editing. Q. X.: Writing – review & editing. N. Q. Z.: Conceptualization, supervision, funding acquisition, writing – review & editing. All the authors have approved the final manuscript.

Use of AI statement

None.

References

[1] Wang, S. W.; Wang, L. G.; Wang, D. S.; Li, Y. D. Recent advances of single-atom catalysts in CO_2 conversion. *Energy Environ. Sci.* **2023**, *16*, 2759–2803.

[2] Dai, F. X.; Zhang, M. M.; Han, J. S.; Li, Z. J.; Feng, S. H.; Xing, J.; Wang, L. Bifunctional core–shell Co-catalyst for boosting photocatalytic CO_2 reduction to CH_4. *Nano Res.* **2024**, *17*, 1259–1266.

[3] Xie, J.; Lu, Z. J.; Feng, Y.; Huang, J. G.; Hu, J. D.; Hao, A. Z.; Cao, Y. L. A small organic molecule strategy for remedying oxygen vacancies by bismuth defects in BiOBr nanosheet with excellent photocatalytic CO_2 reduction. *Nano Res.* **2024**, *17*, 297–306.

[4] Zhang, N. Q.; Zhang, X. X.; Tao, L.; Jiang, P.; Ye, C. L.; Lin, R.; Huang, Z. W.; Li, A.; Pang, D. W.; Yan, H. et al. Silver single-atom catalyst for efficient electrochemical CO_2 reduction synthesized from thermal transformation and surface reconstruction. *Angew. Chem., Int. Ed.* **2021**, *60*, 6170–6176.

[5] Zhang, N. Q.; Zhang, X. X.; Kang, Y. K.; Ye, C. L.; Jin, R.; Yan, H.; Lin, R.; Yang, J. R.; Xu, Q.; Wang, Y. et al. A supported Pd_2 dual-atom site catalyst for efficient electrochemical CO_2 reduction. *Angew. Chem.* **2021**, *133*, 13500–13505.

[6] Ning, S. B.; Ou, H. H.; Li, Y. G.; Lv, C. C.; Wang, S. F.; Wang, D. S.; Ye, J. H. Co^0–$Co^{\delta+}$ interface double-site-mediated C–C coupling for the photothermal conversion of CO_2 into light olefins. *Angew. Chem., Int. Ed.* **2023**, *62*, e202302253.

[7] Chen, S. H.; Ye, C. L.; Wang, Z. W.; Li, P.; Jiang, W. J.; Zhuang, Z. C.; Zhu, J. X.; Zheng, X. B.; Zaman, S.; Ou, H. H. et al. Selective CO_2 reduction to ethylene mediated by adaptive small-molecule engineering of copper-based electrocatalysts. *Angew. Chem., Int. Ed.* **2023**, *62*, e202315621.

[8] Zhang, Z. D.; Zhu, J. X.; Chen, S. H.; Sun, W. M.; Wang, D. S. Liquid fluxional Ga single atom catalysts for efficient electrochemical CO_2 reduction. *Angew. Chem., Int. Ed.* **2023**, *62*, e202215136.

[9] Chang, K.; Zhang, H. C.; Cheng, M. J.; Lu, Q. Application of ceria in CO_2 conversion catalysis. *ACS Catal.* **2020**, *10*, 613–631.

[10] United Nations Environment Programme. Emissions Gap Report 2023: Broken Record—Temperatures hit new highs, yet world fails to cut emissions (again). Nairobi, 2023 [Online]. https://wedocs.unep.org/bitstream/handle/20.500.11822/43922/EGR2023.pdf?sequence=3&isAllowed=y (accessed Apr 15, 2024).

[11] Mac Dowell, N.; Fennell, P. S.; Shah, N.; Maitland, G. C. The role of CO_2 capture and utilization in mitigating climate change. *Nat. Climate Change* **2017**, *7*, 243–249.

[12] Gao, W. L.; Liang, S. Y.; Wang, R. J.; Jiang, Q.; Zhang, Y.; Zheng, Q. W.; Xie, B. Q.; Toe, C. Y.; Zhu, X. C.; Wang, J. Y. et al. Industrial carbon dioxide capture and utilization: State of the art and future challenges. *Chem. Soc. Rev.* **2020**, *49*, 8584–8686.

[13] Zhang, S. H.; Shen, Y.; Shao, P. J.; Chen, J. M.; Wang, L. D. Kinetics, thermodynamics, and mechanism of a novel biphasic solvent for CO_2 capture from flue gas. *Environ. Sci. Technol.* **2018**, *52*, 3660–3668.

[14] Li, L. C.; Zhang, N. Q.; Wu, Z. Y.; Miyazaki, S.; Toyao, T.; Maeno, Z.; Shimizu, K. I. Rb-Ni/Al_2O_3 as dual functional material for continuous CO_2 capture and selective hydrogenation to CO. *Chem. Eng. J.* **2023**, *477*, 147199.

[15] Li, L. C.; Miyazaki, S.; Wu, Z. Y.; Toyao, T.; Selyanchyn, R.; Maeno, Z.; Fujikawa, S.; Shimizu, K. I. Continuous direct air capture and methanation using combined system of membrane-based CO_2 capture and Ni-Ca based dual functional materials. *Appl. Catal. B: Environ.* **2023**, *339*, 123151.

[16] Li, L. C.; Miyazaki, S.; Yasumura, S.; Ting, K. W.; Toyao, T.; Maeno, Z.; Shimizu, K. I. Continuous CO_2 capture and selective hydrogenation to CO over Na-promoted Pt nanoparticles on Al_2O_3. *ACS Catal.* **2022**, *12*, 2639–2650.

[17] Lin, Q. Y.; Zhang, X.; Wang, T.; Zheng, C. H.; Gao, X. Technical perspective of carbon capture, utilization, and storage. *Engineering* **2022**, *14*, 27–32.

[18] Zhang, J. P.; Li, Z. W.; Zhang, Z. H.; Feng, K.; Yan, B. H. Can thermocatalytic transformations of captured CO_2 reduce CO_2 emissions. *Appl. Energy* **2021**, *281*, 116076.

[19] Keith, D. W.; Holmes, G.; St. Angelo, D.; Heidel, K. A process for capturing CO_2 from the atmosphere. *Joule* **2018**, *2*, 1573–1594.

[20] Wang, W. H.; Himeda, Y.; Muckerman, J. T.; Manbeck, G. F.; Fujita, E. CO_2 hydrogenation to formate and methanol as an alternative to photo- and electrochemical CO_2 reduction. *Chem. Rev.* **2015**, *115*, 12936–12973.

[21] Jiang, X.; Nie, X. W.; Guo, X. W.; Song, C. S.; Chen, J. G. Recent advances in carbon dioxide hydrogenation to methanol via heterogeneous catalysis. *Chem. Rev.* **2020**, *120*, 7984–8034.

[22] Wang, Z.; Sun, Z. H.; Yin, H.; Wei, H. H.; Peng, Z. C.; Pang, Y. X.; Jia, G. H.; Zhao, H. T.; Pang, C. H.; Yin, Z. Y. The role of machine learning in carbon neutrality: Catalyst property prediction, design, and synthesis for carbon dioxide reduction. *eScience* **2023**, *3*, 100136.

[23] Zhou, J.; Liu, H.; Wang, H. Q. Photothermal catalysis for CO_2 conversion. *Chin. Chem. Lett.* **2023**, *34*, 107420.

[24] Liu, Q. G.; Yang, X. F.; Li, L.; Miao, S.; Li, Y.; Li, Y. Q.; Wang, X. K.; Huang, Y. Q.; Zhang, T. Direct catalytic hydrogenation of CO_2 to formate over a schiff-base-mediated gold nanocatalyst. *Nat. Commun.* **2017**, *8*, 1407.

[25] Ye, X.; Ma, J. G.; Yu, W. G.; Pan, X. L.; Yang, C. Y.; Wang, C.; Liu, Q. G.; Huang, Y. Q. Construction of bifunctional single-atom catalysts on the optimized β-Mo_2C surface for highly selective hydrogenation of CO_2 into ethanol. *J. Energy Chem.* **2022**, *67*, 184–192.

[26] Ding, X. X.; Zhu, M. H.; Sun, B.; Yang, Z. X.; Han, Y. F. An overview on dynamic phase transformation and surface reconstruction of iron catalysts for catalytic hydrogenation of CO_x for hydrocarbons. *ACS Catal.* **2024**, *14*, 6137–6168.

[27] Galadima, A.; Muraza, O. Catalytic thermal conversion of CO_2 into fuels: Perspective and challenges. *Renew. Sustain. Energy Rev.* **2019**, *115*, 109333.

[28] Zhu, P.; Xiong, X.; Wang, D. S. Regulations of active moiety in single atom catalysts for electrochemical hydrogen evolution reaction. *Nano Res.* **2022**, *15*, 5792–5815.

[29] Ma, R.; Sun, J.; Li, D. H.; Wei, J. J. Review of synergistic photo-thermo-catalysis: Mechanisms, materials and applications. *Int. J. Hydrogen Energy* **2020**, *45*, 30288–30324.

[30] Fu, J. W.; Jiang, K. X.; Qiu, X. Q.; Yu, J. G.; Liu, M. Product selectivity of photocatalytic CO_2 reduction reactions. *Mater. Today* **2020**, *32*, 222–243.

[31] Zeng, Y.; Zhao, M. T.; Zeng, H. L.; Jiang, Q.; Ming, F. W.; Xi, K.; Wang, Z. C.; Liang, H. F. Recent progress in advanced catalysts for electrocatalytic hydrogenation of organics in aqueous conditions. *eScience* **2023**, *3*, 100156.

[32] Wang, M.; Luo, J. S. A coupled electrochemical system for CO_2 capture, conversion and product purification. *eScience* **2023**, *3*, 100155.

[33] Zhao, X. X.; Guan, J. R.; Li, J. Z.; Li, X.; Wang, H. Q.; Huo, P. W.; Yan, Y. S. CeO_2/3D g-C_3N_4 heterojunction deposited with Pt cocatalyst for enhanced photocatalytic CO_2 reduction. *Appl. Surf. Sci.* **2021**, *537*, 147891.

[34] Yang, C.; Li, Q.; Xia, Y.; Lv, K. L.; Li, M. Enhanced visible-light photocatalytic CO_2 reduction performance of $Znln_2S_4$ microspheres by using CeO_2 as cocatalyst. *Appl. Surf. Sci.* **2019**, *464*, 388–395.

[35] Mahyoub, S. A.; Hezam, A.; Qaraah, F. A.; Namratha, K.; Nayan, M. B.; Drmosh, Q. A.; Ponnamma, D.; Byrappa, K. Surface plasmonic resonance and Z-scheme charge transport synergy in three-dimensional flower-like Ag–CeO_2–ZnO heterostructures for highly improved photocatalytic CO_2 reduction. *ACS Appl. Energy Mater.* **2021**, *4*, 3544–3554.

[36] Yaseen, M.; Jiang, H. P.; Li, J. H.; Yu, X. H.; Ashfaq Ahmad, M.; Nauman Ali, R.; Wang, L. L.; Yang, J.; Liu, Q. Q. Synergistic effect of Z-scheme and oxygen vacancy of CeO_2/WO_3 heterojunction for enhanced CO_2 reduction activity. *Appl. Surf. Sci.* **2023**, *631*, 157360.

[37] Yaashikaa, P. R.; Senthil Kumar, P.; Varjani, S. J.; Saravanan, A. A review on photochemical, biochemical and electrochemical transformation of CO_2 into value-added products. *J. CO_2 Util.* **2019**, *33*, 131–147.

[38] Overa, S.; Ko, B. H.; Zhao, Y. R.; Jiao, F. Electrochemical approaches for CO_2 conversion to chemicals: A journey toward practical applications. *Acc. Chem. Res.* **2022**, *55*, 638–648.

[39] Lee, W. J.; Li, C. E.; Prajitno, H.; Yoo, J.; Patel, J.; Yang, Y. X.; Lim, S. Recent trend in thermal catalytic low temperature CO_2 methanation: A critical review. *Catal. Today* **2021**, *368*, 2–19.

[40] Li, L. C.; Chen, D. T.; Anzai, A.; Zhang, N. Q.; Kang, Y. K.; Qian, Y. C.; Du, P. F.; Fakir, A. A. E.; Tayao, T.; Shimizu, K. *Operando* spectroscopic studies on redox mechanism for CO_2 hydrogenation to CO on In_2O_3 catalysts. *J. Catal.*, in press, DOI: 10.1016/j.jcat.2024.115762.

[41] Wang, W. X.; Zhao, S. Z.; Tang, X. L.; Chen, C. Q.; Yi, H. H. Electrothermal catalysis for heterogeneous reaction: Mechanisms and design strategies. *Chem. Eng. J.* **2023**, *455*, 140272.

[42] Ye, L. T.; Xie, K. High-temperature electrocatalysis and key materials in solid oxide electrolysis cells. *J. Energy Chem.* **2021**, *54*, 736–745.

[43] Lv, C. C.; Bai, X. H.; Ning, S. B.; Song, C. X.; Guan, Q. Q.; Liu, B.; Li, Y. G.; Ye, J. H. Nanostructured materials for photothermal carbon dioxide hydrogenation: Regulating solar utilization and catalytic performance. *ACS Nano* **2023**, *17*, 1725–1738.

[44] Li, J. W.; Dou, L. G.; Gao, Y.; Hei, X. T.; Yu, F.; Shao, T. Revealing the active sites of the structured Ni-based catalysts for one-step CO_2/CH_4 conversion into oxygenates by plasma-catalysis. *J. CO_2 Util.* **2021**, *52*, 101675.

[45] Luo, S. Q.; Ren, X. H.; Lin, H. W.; Song, H.; Ye, J. H. Plasmonic photothermal catalysis for solar-to-fuel conversion: Current status and prospects. *Chem. Sci.* **2021**, *12*, 5701–5719.

[46] Zhang, X.; Xu, Y.; Liu, Y.; Niu, L.; Diao, Y. N.; Gao, Z. R.; Chen,

B. B.; Xie, J. L.; Bi, M.; Wang, M. et al. A novel Ni–MoC_xO_y interfacial catalyst for syngas production via the chemical looping dry reforming of methane. *Chem* **2023**, *9*, 102–116.

[47] Zheng, T. T.; Jiang, K.; Wang, H. T. Recent advances in electrochemical CO_2-to-CO conversion on heterogeneous catalysts. *Adv. Mater.* **2018**, *30*, 1802066.

[48] George, A.; Shen, B. X.; Craven, M.; Wang, Y. L.; Kang, D. R.; Wu, C. F.; Tu, X. A review of non-thermal plasma technology: A novel solution for CO_2 conversion and utilization. *Renew. Sustain. Energy Rev.* **2021**, *135*, 109702.

[49] Zhu, Y. F.; Xie, B. Q.; Amal, R.; Lovell, E. C.; Scott, J. Light-enhanced conversion of CO_2 to light olefins: Basis in thermal catalysis, current progress, and future prospects. *Small Struct.* **2023**, *4*, 2200285.

[50] Wang, Z. Q.; Yang, Z. Q.; Fang, R. M.; Yan, Y. F.; Ran, J. Y.; Zhang, L. A State-of-the-art review on action mechanism of photothermal catalytic reduction of CO_2 in full solar spectrum. *Chem. Eng. J.* **2022**, *429*, 132322.

[51] Wang, Y. Y.; Zhou, Q. X.; Zhu, Y. F.; Xu, D. S. High efficiency reduction of CO_2 to CO and CH_4 via photothermal synergistic catalysis of lead-free perovskite $Cs_3Sb_2I_9$. *Appl. Catal. B: Environ.* **2021**, *294*, 120236.

[52] Zhao, J. Q.; Guo, X. D.; Shi, R.; Waterhouse, G. I. N.; Zhang, X. R.; Dai, Q.; Zhang, T. R. NiFe nanoalloys derived from layered double hydroxides for photothermal synergistic reforming of CH_4 with CO_2. *Adv. Funct. Mater.* **2022**, *32*, 2204056.

[53] Wang, Z. Q.; Yang, Z. Q.; Kadirova, Z. C.; Guo, M.; Fang, R. M.; He, J.; Yan, Y. F.; Ran, J. Y. Photothermal functional material and structure for photothermal catalytic CO_2 reduction: Recent advance, application and prospect. *Coord. Chem. Rev.* **2022**, *473*, 214794.

[54] Xiao, Z. R.; Li, P.; Zhang, H.; Zhang, S. L.; Tan, X. Y.; Ye, F.; Gu, J. M.; Zou, J. J.; Wang, D. S. A comprehensive review on photo-thermal co-catalytic reduction of CO_2 to value-added chemicals. *Fuel* **2024**, *362*, 130906.

[55] Guo, R. T.; Xia, C.; Bi, Z. X.; Zhang, Z. R.; Pan, W. G. Recent progress of photothermal effect on photocatalytic reduction of CO_2. *Fuel Process. Technol.* **2023**, *241*, 107617.

[56] Huang, X. B.; Zhang, K. Y.; Peng, B. X.; Wang, G.; Muhler, M.; Wang, F. Ceria-based materials for thermocatalytic and photocatalytic organic synthesis. *ACS Catal.* **2021**, *11*, 9618–9678.

[57] Yan, H.; Zhang, N. Q.; Wang, D. S. Highly efficient CeO_2-supported noble-metal catalysts: From single atoms to nanoclusters. *Chem Catal.* **2022**, *2*, 1594–1623.

[58] Montini, T.; Melchionna, M.; Monai, M.; Fornasiero, P. Fundamentals and catalytic applications of CeO_2-based materials. *Chem. Rev.* **2016**, *116*, 5987–6041.

[59] Dong, F.; Liang, X.; Zhang, Z. D.; Yin, H. B.; Wang, D. S.; Li, J. H.; Li, Y. D. Atomic Pt sites anchored in the interface between grains on vacancy-enriched CeO_2 nanosheets: One-step precursor combustion synthesis. *Adv. Mater.* **2024**, *36*, 2401055.

[60] Zhang, N. Q.; Tong, J. H.; Miyazaki, S.; Zhao, S. R.; Kubota, H.; Jing, Y.; Mine, S.; Toyao, T.; Shimizu, K. I. Mechanism of NH_3-SCR over P/CeO_2 catalysts investigated by *operando* spectroscopies. *Environ. Sci. Technol.* **2023**, *57*, 16289–16295.

[61] Zhang, N. Q.; Qian, Y. C.; Toyao, T.; Shimizu, K. I. Continuous unsteady-state De-NO_x system via tandem water-gas shift, NH_3 synthesis, and NH_3-SCR under periodic lean/rich conditions. *Environ. Sci. Technol.* **2023**, *57*, 19584–19593.

[62] Zhang, N. Q.; Yan, H.; Li, L. C.; Wu, R.; Song, L. Y.; Zhang, G. Z.; Liang, W. J.; He, H. Use of rare earth elements in single-atom site catalysis: A critical review—Commemorating the 100th anniversary of the birth of academician Guangxian Xu. *J. Rare Earths* **2021**, *39*, 233–242.

[63] Pang, D. W.; Li, W.; Zhang, N. Q.; He, H.; Mao, S. C.; Chen, Y. H.; Cao, L. W.; Li, C.; Li, A.; Han, X. D. Direct observation of oxygen vacancy formation and migration over ceria surface by *in situ* environmental transmission electron microscopy. *J. Rare Earths* **2024**, *42*, 676–682.

[64] Chitsazi, H.; Zhang, N. Q.; Li, L. C.; Liu, X. J.; Wu, R.; He, J. D.; Song, L. Y.; He, H. *In-situ* DRIFT assessment on strengthening effect of cerium over FeO_x/TiO_2 catalyst for selective catalytic reduction of NO_x with NH_3. *J. Rare Earths* **2021**, *39*, 526–531.

[65] Xu, Q.; Cheng, X. W.; Zhang, N. Q.; Tu, Y.; Wu, L. H.; Pan, H. B.; Hu, J.; Ding, H. H.; Zhu, J. F.; Li, Y. D. Unraveling the advantages of Pd/CeO_2 single-atom catalysts in the NO + CO reaction by model catalysts. *Nano Res.* **2023**, *16*, 8882–8892.

[66] Xie, S. H.; Liu, L. P.; Lu, Y.; Wang, C. Y.; Cao, S. F.; Diao, W. J.; Deng, J. G.; Tan, W.; Ma, L.; Ehrlich, S. N. et al. Pt atomic single-layer catalyst embedded in defect-enriched ceria for efficient CO oxidation. *J. Am. Chem. Soc.* **2022**, *144*, 21255–21266.

[67] Yan, H.; Qin, X. T.; Liu, J. C.; Cai, L. H.; Xu, P.; Song, J. J.; Ma, C.; Wang, W. W.; Jin, Z.; Jia, C. J. Releasing the limited catalytic activity of CeO_2-supported noble metal catalysts via UV-induced deep dechlorination. *J. Catal.* **2022**, *413*, 703–712.

[68] Li, Q. Q.; Song, L. P.; Liang, Z.; Sun, M. Z.; Wu, T.; Huang, B. L.; Luo, F.; Du, Y. P.; Yan, C. H. A review on CeO_2-based electrocatalyst and photocatalyst in energy conversion. *Adv. Energy Sustain. Res.* **2021**, *2*, 2000063.

[69] Tran, D. P. H.; Pham, M. T.; Bui, X. T.; Wang, Y. F.; You, S. J. CeO_2 as a photocatalytic material for CO_2 conversion: A review. *Solar Energy* **2022**, *240*, 443–466.

[70] Zhang, Y.; Zhao, S. N.; Feng, J.; Song, S. Y.; Shi, W. D.; Wang, D.; Zhang, H. J. Unraveling the physical chemistry and materials science of CeO_2-based nanostructures. *Chem* **2021**, *7*, 2022–2059.

[71] Yang, Y.; Zhao, S. H.; Cui, L. F.; Bi, F. K.; Zhang, Y. N.; Liu, N.; Wang, Y. X.; Liu, F. D.; He, C.; Zhang, X. D. Recent advancement and future challenges of photothermal catalysis for VOCs elimination: From catalyst design to applications. *Green Energy Environ.* **2023**, *8*, 654–672.

[72] Liu, H. M.; Shi, L. Z.; Zhang, Q. J.; Qi, P.; Zhao, Y. H.; Meng, Q. R.; Feng, X. Q.; Wang, H.; Ye, J. H. Photothermal catalysts for hydrogenation reactions. *Chem. Commun.* **2021**, *57*, 1279–1294.

[73] Zhang, J. Q.; Chen, H. J.; Duan, X. G.; Sun, H. Q.; Wang, S. B. Photothermal catalysis: From fundamentals to practical applications. *Mater. Today* **2023**, *68*, 234–253.

[74] Mateo, D.; Cerrillo, J. L.; Durini, S.; Gascon, J. Fundamentals and applications of photo-thermal catalysis. *Chem. Soc. Rev.* **2021**, *50*, 2173–2210.

[75] Song, X. Y.; Shan, X. C.; Xue, H.; Li, X.; Liu, R. Z.; Kong, J. R.; Zuo, Z. H.; Su, X. W.; Zhang, Q. Z.; Yin, Y. G. et al. Advances in photothermal catalysis: Mechanisms, materials, and environmental applications. *ACS Appl. Nano Mater.*, in press, DOI: 10.1021/acsanm.4c00598.

[76] Coronado, J. M.; Fresno, F.; Hernández-Alonso, M. D.; Portela, R. *Design of Advanced Photocatalytic Materials for Energy and Environmental Applications*; Springer: London, 2013.

[77] Fujishima, A.; Honda, K. Electrochemical photolysis of water at a semiconductor electrode. *Nature* **1972**, *238*, 37–38.

[78] Melsheimer, J.; Guo, W.; Ziegler, D.; Wesemann, M.; Schlögl, R. Methanation of carbon dioxide over Ru/titania at room temperature: Explorations for a photoassisted catalytic reaction. *Catal. Lett.* **1991**, *11*, 157–168.

[79] Anikeev, V. I.; Parmon, V. N.; Kirillov, V. A.; Zamaraev, K. I. Theoretical and experimental studies of solar catalytic power plants based on reversible reactions with participation of methane and synthesis gas. *Int. J. Hydrogen Energy* **1990**, *15*, 275–286.

[80] Christopher, P.; Xin, H. L.; Linic, S. Visible-light-enhanced catalytic oxidation reactions on plasmonic silver nanostructures. *Nat. Chem.* **2011**, *3*, 467–472.

[81] Langhammer, C.; Larsson, E. M. Nanoplasmonic *in situ* spectroscopy for catalysis applications. *ACS Catal.* **2012**, *2*, 2036–2045.

[82] Trovarelli, A. Catalytic properties of ceria and CeO_2-containing materials. *Catal. Rev.* **1996**, *38*, 439–520.
[83] Jiang, D.; Wang, W. Z.; Sun, S. M.; Zhang, L.; Zheng, Y. L. Equilibrating the plasmonic and catalytic roles of metallic nanostructures in photocatalytic oxidation over Au-modified CeO_2. *ACS Catal.* **2015**, *5*, 613–621.
[84] Zou, J. S.; Si, Z. C.; Cao, Y. D.; Ran, R.; Wu, X. D.; Weng, D. Localized surface plasmon resonance assisted photothermal catalysis of CO and toluene oxidation over Pd–CeO_2 catalyst under visible light irradiation. *J. Phys. Chem. C* **2016**, *120*, 29116–29125.
[85] Lee, J.; Ryou, Y.; Chan, X.; Kim, T. J.; Kim, D. H. How Pt interacts with CeO_2 under the reducing and oxidizing environments at elevated temperature: The origin of improved thermal stability of Pt/CeO_2 compared to CeO_2. *J. Phys. Chem. C* **2016**, *120*, 25870–25879.
[86] Zhong, H. X.; Wei, Y.; Yue, Y. Z.; Zhang, L. H.; Liu, Y. Preparation of core–shell Ag@CeO_2 nanocomposite by LSPR photothermal induced interface reaction. *Nanotechnology* **2016**, *27*, 135701.
[87] Zhang, Q.; Mao, M. Y.; Li, Y. Z.; Yang, Y.; Huang, H.; Jiang, Z. K.; Hu, Q. Q.; Wu, S. W.; Zhao, X. J. Novel photoactivation promoted light-driven CO_2 reduction by CH_4 on Ni/CeO_2 nanocomposite with high light-to-fuel efficiency and enhanced stability. *Appl. Catal. B: Environ.* **2018**, *239*, 555–564.
[88] Quan, F. J.; Zhan, G. M.; Mao, C. L.; Ai, Z. H.; Jia, F. L.; Zhang, L. Z.; Gu, H. G.; Liu, S. Y. Efficient light-driven CO_2 hydrogenation on Ru/CeO_2 catalysts. *Catal. Sci. Technol.* **2018**, *8*, 6503–6510.
[89] Bernal, S.; Calvino, J. J.; Cauqui, M. A.; Gatica, J. M.; Larese, C.; Pérez Omil, J. A.; Pintado, J. M. Some recent results on metal/support interaction effects in NM/CeO_2 (NM: noble metal) catalysts. *Catal. Today* **1999**, *50*, 175–206.
[90] Zhu, L. L.; Gao, M. M.; Nuo Peh, C. K.; Wei Ho, G. Solar-driven photothermal nanostructured materials designs and prerequisites for evaporation and catalysis applications. *Mater. Horiz.* **2018**, *5*, 323–343.
[91] Jiang, H. J.; Liu, X. H.; Wang, D. W.; Qiao, Z. N.; Wang, D.; Huang, F.; Peng, H. Y.; Hu, C. Q. Designing high-efficiency light-to-thermal conversion materials for solar desalination and photothermal catalysis. *J. Energy Chem.* **2023**, *79*, 581–600.
[92] Xie, B. Q.; Lovell, E.; Tan, T. H.; Jantarang, S.; Yu, M. Y.; Scott, J.; Amal, R. Emerging material engineering strategies for amplifying photothermal heterogeneous CO_2 catalysis. *J. Energy Chem.* **2021**, *59*, 108–125.
[93] Hong, J. N.; Xu, C. Y.; Deng, B. W.; Gao, Y.; Zhu, X.; Zhang, X. H.; Zhang, Y. W. Photothermal chemistry based on solar energy: From synergistic effects to practical applications. *Adv. Sci.* **2022**, *9*, 2103926.
[94] Keller, N.; Ivanez, J.; Highfield, J.; Ruppert, A. M. Photo-/thermal synergies in heterogeneous catalysis: Towards low-temperature (solar-driven) processing for sustainable energy and chemicals. *Appl. Catal. B: Environ.* **2021**, *296*, 120320.
[95] Tian, J. D.; Han, R.; Guo, Q. S.; Zhao, Z.; Sha, N. Direct conversion of CO_2 into hydrocarbon solar fuels by a synergistic photothermal catalysis. *Catalysts* **2022**, *12*, 612.
[96] Xu, J.; Wang, Y.; Wang, K.; Zhao, M.; Zhang, R.; Cui, W. J.; Liu, L.; Bootharaju, M. S.; Kim, J. H.; Hyeon, T. et al. Single-atom Rh on high-index CeO_2 facet for highly enhanced catalytic CO oxidation. *Angew. Chem.* **2023**, *135*, e202302877.
[97] Song, S. Y.; Wang, X.; Zhang, H. J. CeO_2-encapsulated noble metal nanocatalysts: Enhanced activity and stability for catalytic application. *NPG Asia Mater.* **2015**, *7*, e179.
[98] Sivan, S. E.; Kang, K. H.; Han, S. J.; Francis Ngome Okello, O.; Choi, S. Y.; Sudheeshkumar, V.; Scott, R. W. J.; Chae, H. J.; Park, S.; Lee, U. H. Facile MOF-derived one-pot synthetic approach toward Ru single atoms, nanoclusters, and nanoparticles dispersed on CeO_2 supports for enhanced ammonia synthesis. *J. Catal.* **2022**, *408*, 316–328.
[99] Li, L. C.; Zhang, N. Q. Atomic dispersion of bulk/nano metals to atomic-sites catalysts and their application in thermal catalysis. *Nano Res.* **2023**, *16*, 6380–6401.
[100] Zhang, N. Q.; Ye, C. L.; Yan, H.; Li, L. C.; He, H.; Wang, D. S.; Li, Y. D. Single-atom site catalysts for environmental catalysis. *Nano Res.* **2020**, *13*, 3165–3182.
[101] Zhuang, J. H.; Wang, D. S. Recent advances of single-atom alloy catalyst: Properties, synthetic methods and electrocatalytic applications. *Mater. Today Catal.* **2023**, *2*, 100009.
[102] Zhou, A. W.; Wang, D. S.; Li, Y. D. Hollow microstructural regulation of single-atom catalysts for optimized electrocatalytic performance. *Microstructures* **2022**, *2*, 2022005.
[103] Guan, S. Y.; Yuan, Z. L.; Zhuang, Z. C.; Zhang, H. H.; Wen, H.; Fan, Y. P.; Li, B. J.; Wang, D. S.; Liu, B. Z. Why do single-atom alloys catalysts outperform both single-atom catalysts and nanocatalysts on MXene. *Angew. Chem., Int. Ed.* **2024**, *63*, e202316550.
[104] Zhu, C. X.; Yang, J. R.; Zhang, J. W.; Wang, X. Q.; Gao, Y.; Wang, D. S.; Pan, H. G. Single-atom materials: The application in energy conversion. *Interdiscip. Mater.* **2024**, *3*, 74–86.
[105] Wang, X. Y.; Pan, Y. Z.; Yang, J. R.; Li, W. H.; Gan, T.; Pan, Y. M.; Tang, H. T.; Wang, D. S. Single-atom iron catalyst as an advanced redox mediator for anodic oxidation of organic electrosynthesis. *Angew. Chem., Int. Ed.* **2024**, *63*, e202404295.
[106] Yang, J. R.; Zhu, C. X.; Li, W. H.; Zheng, X. S.; Wang, D. S. Organocatalyst supported by a single-atom support accelerates both electrodes used in the chlor-alkali industry via modification of non-covalent interactions. *Angew. Chem., Int. Ed.* **2024**, *63*, e202314382.
[107] Li, W. H.; Ye, B. C.; Yang, J. R.; Wang, Y.; Yang, C. J.; Pan, Y. M.; Tang, H. T.; Wang, D. S.; Li, Y. D. A single-atom cobalt catalyst for the fluorination of acyl chlorides at parts-per-million catalyst loading. *Angew. Chem., Int. Ed.* **2022**, *61*, e202209749.
[108] Chen, Y. J.; Jiang, B.; Hao, H. G.; Li, H. J.; Qiu, C. Y.; Liang, X.; Qu, Q. Y.; Zhang, Z. D.; Gao, R.; Duan, D. M. et al. Atomic-level regulation of cobalt single-atom nanozymes: Engineering high-efficiency catalase mimics. *Angew. Chem., Int. Ed.* **2023**, *62*, e202301879.
[109] Tang, H. T.; Zhou, H. Y.; Pan, Y. M.; Zhang, J. L.; Cui, F. H.; Li, W. H.; Wang, D. S. Single-atom manganese-catalyzed oxygen evolution drives the electrochemical oxidation of silane to silanol. *Angew. Chem., Int. Ed.* **2024**, *63*, e202315032.
[110] Li, Y. P.; Niu, S. W.; Liu, P. G.; Pan, R. R.; Zhang, H. K.; Ahmad, N.; Shi, Y.; Liang, X.; Cheng, M. Y.; Chen, S. H. et al. Ruthenium nanoclusters and single atoms on α-MoC/N-doped carbon achieves low-input/input-free hydrogen evolution via decoupled/coupled hydrazine oxidation. *Angew. Chem., Int. Ed.* **2024**, *63*, e202316755.
[111] Hu, Y. M.; Chao, T. T.; Li, Y. P.; Liu, P. G.; Zhao, T. H.; Yu, G.; Chen, C.; Liang, X.; Jin, H. L.; Niu, S. W. et al. Cooperative Ni(Co)-Ru-P sites activate dehydrogenation for hydrazine oxidation assisting self-powered H_2 production. *Angew. Chem., Int. Ed.* **2023**, *62*, e202308800.
[112] Wang, Y.; Wu, J.; Tang, S. H.; Yang, J. R.; Ye, C. L.; Chen, J.; Lei, Y. P.; Wang, D. Synergistic Fe–Se atom pairs as bifunctional oxygen electrocatalysts boost low-temperature rechargeable Zn-air battery. *Angew. Chem., Int. Ed.* **2023**, *62*, e202219191.
[113] Han, A. L.; Sun, W. M.; Wan, X.; Cai, D. D.; Wang, X. J.; Li, F.; Shui, J. L.; Wang, D. S. Construction of Co_4 atomic clusters to enable Fe–N_4 motifs with highly active and durable oxygen reduction performance. *Angew. Chem., Int. Ed.* **2023**, *62*, e202303185.
[114] Guan, S. Y.; Yuan, Z. L.; Zhao, S. Q.; Zhuang, Z. C.; Zhang, H. H.; Shen, R. F.; Fan, Y. P.; Li, B. J.; Wang, D. S.; Liu, B. Z. Efficient hydrogen generation from ammonia borane hydrolysis on a tandem ruthenium-platinum-titanium catalyst. *Angew. Chem., Int. Ed.* **2024**, *63*, e202408193.
[115] Qiu, W. B.; Qin, S. M.; Li, Y. B.; Cao, N.; Cui, W. R.; Zhang, Z. D.; Zhuang, Z. C.; Wang, D. S.; Zhang, Y. Overcoming electrostatic

interaction via pulsed electroreduction for boosting the electrocatalytic urea synthesis. *Angew. Chem., Int. Ed.* **2024**, *63*, e202402684.

[116] Lv, L. Y.; Tan, H.; Kong, Y.; Tang, B.; Ji, Q. Q.; Liu, Y. Y.; Wang, C.; Zhuang, Z. C.; Wang, H. J.; Ge, M. et al. Breaking the scaling relationship in C–N coupling via the doping effects for efficient urea electrosynthesis. *Angew. Chem., Int. Ed.* **2024**, *63*, e202401943.

[117] Tao, Y.; Guan, J. P.; Zhang, J.; Hu, S. Y.; Ma, R. Z.; Zheng, H. R.; Gong, J. X.; Zhuang, Z. C.; Liu, S. J.; Ou, H. H. et al. Ruthenium single atomic sites surrounding the support pit with exceptional photocatalytic activity. *Angew. Chem., Int. Ed.* **2024**, *63*, e202400625.

[118] Mu, X. Q.; Liu, S. L.; Zhang, M. Y.; Zhuang, Z. C.; Chen, D.; Liao, Y. R.; Zhao, H. Y.; Mu, S. C.; Wang, D. S.; Dai, Z. H. Symmetry-broken Ru nanoparticles with parasitic Ru-Co dual-single atoms overcome the volmer step of alkaline hydrogen oxidation. *Angew. Chem., Int. Ed.* **2024**, *63*, e202319618.

[119] Zhang, Y. D.; Sun, Y. J.; Wang, Q. Y.; Zhuang, Z. C.; Ma, Z. T.; Liu, L. M.; Wang, G. M.; Wang, D. S.; Zheng, X. S. Synergy of photogenerated electrons and holes toward efficient photocatalytic urea synthesis from CO_2 and N_2. *Angew. Chem., Int. Ed.* **2024**, *63*, e202405637.

[120] Zhao, J.; Zhang, Y. X.; Zhuang, Z. C.; Deng, Y. T.; Gao, G.; Li, J. Y.; Meng, A. L.; Li, G. C.; Wang, L.; Li, Z. J. et al. Tailoring d–p orbital hybridization to decipher the essential effects of heteroatom substitution on redox kinetics. *Angew. Chem.* **2024**, *136*, e202404968.

[121] Yang, J. R.; Zhu, C. X.; Wang, D. S. A simple organo-electrocatalysis system for the chlor-related industry. *Angew. Chem., Int. Ed.* **2024**, *63*, e202406883.

[122] Chen, F. J.; Mu, X. Q.; Zhou, J. L.; Wang, S. C.; Liu, Z. Y.; Zhou, D. Y.; Liu, S. L.; Wang, D. S.; Dai, Z. H. Engineering the active sites of MOF-derived catalysts: From oxygen activation to activate metal-air batteries. *Chin. J. Chem*., in press, DOI: 10.1002/cjoc.202400332.

[123] Guo, Y. J.; Liu, Z. Y.; Zhou, D. Y.; Zhang, M. Y.; Zhang, Y.; Li, R. Z.; Liu, S. L.; Wang, D. S.; Dai, Z. H. Competition and synergistic effects of Ru-based single-atom and cluster catalysts in electrocatalytic reactions. *Sci. China Mater.* **2024**, *67*, 1706–1720.

[124] Zhang, Y. F.; Liu, L. S.; Li, Y. X.; Mu, X. Q.; Mu, S. C.; Liu, S. L.; Dai, Z. H. Strong synergy between physical and chemical properties: Insight into optimization of atomically dispersed oxygen reduction catalysts. *J. Energy Chem.* **2024**, *91*, 36–49.

[125] Wang, S. C.; Zhang, M. Y.; Mu, X. Q.; Liu, S. L.; Wang, D. S.; Dai, Z. H. Atomically dispersed multi-site catalysts: Bifunctional oxygen electrocatalysts boost flexible zinc-air battery performance. *Energy Environ. Sci.* **2024**, *17*, 4847–4870.

[126] Li, Z.; Ji, S. F.; Liu, Y. W.; Cao, X.; Tian, S. B.; Chen, Y. J.; Niu, Z. Q.; Li, Y. D. Well-defined materials for heterogeneous catalysis: From nanoparticles to isolated single-atom sites. *Chem. Rev.* **2020**, *120*, 623–682.

[127] Chen, X. W.; Peng, M.; Xiao, D. Q.; Liu, H. Y.; Ma, D. Fully exposed metal clusters: Fabrication and application in alkane dehydrogenation. *ACS Catal.* **2022**, *12*, 12720–12743.

[128] Rong, H. P.; Ji, S. F.; Zhang, J. T.; Wang, D. S.; Li, Y. D. Synthetic strategies of supported atomic clusters for heterogeneous catalysis. *Nat. Commun.* **2020**, *11*, 5884.

[129] Shin, S.; Haaring, R.; So, J.; Choi, Y.; Lee, H. Highly durable heterogeneous atomic catalysts. *Acc. Chem. Res.* **2022**, *55*, 1372–1382.

[130] Babucci, M.; Guntida, A.; Gates, B. C. Atomically dispersed metals on well-defined supports including zeolites and metal-organic frameworks: Structure, bonding, reactivity, and catalysis. *Chem. Rev.* **2020**, *120*, 11956–11985.

[131] Tian, S. B.; Wang, B. X.; Gong, W. B.; He, Z. Z.; Xu, Q.; Chen, W. X.; Zhang, Q. H.; Zhu, Y. Q.; Yang, J. R.; Fu, Q. et al. Dual-atom Pt heterogeneous catalyst with excellent catalytic performances for the selective hydrogenation and epoxidation. *Nat. Commun.* **2021**, *12*, 3181.

[132] Yang, J. R.; Li, W. H.; Xu, K. N.; Tan, S. D.; Wang, D. S.; Li, Y. D. Regulating the tip effect on single-atom and cluster catalysts: Forming reversible oxygen species with high efficiency in chlorine evolution reaction. *Angew. Chem.* **2022**, *134*, e202200366.

[133] Nie, L.; Mei, D. H.; Xiong, H. F.; Peng, B.; Ren, Z. B.; Hernandez, X. I. P.; DeLaRiva, A.; Wang, M.; Engelhard, M. H.; Kovarik, L. et al. Activation of surface lattice oxygen in single-atom Pt/CeO_2 for low-temperature CO oxidation. *Science* **2017**, *358*, 1419–1423.

[134] Zhou, X.; Li, K.; Lin, Y. X.; Song, L.; Liu, J. C.; Liu, Y.; Zhang, L. L.; Wu, Z. J.; Song, S. Y.; Li, J. et al. A single-atom manipulation approach for synthesis of atomically mixed nanoalloys as efficient catalysts. *Angew. Chem., Int. Ed.* **2020**, *59*, 13568–13574.

[135] Konsolakis, M.; Lykaki, M. Facet-dependent reactivity of ceria nanoparticles exemplified by CeO_2-based transition metal catalysts: A critical review. *Catalysts* **2021**, *11*, 452.

[136] Zhao, S. Z.; Kang, D. J.; Liu, Y. P.; Wen, Y. F.; Xie, X. Z.; Yi, H. H.; Tang, X. L. Spontaneous formation of asymmetric oxygen vacancies in transition-metal-doped CeO_2 nanorods with improved activity for carbonyl sulfide hydrolysis. *ACS Catal.* **2020**, *10*, 11739–11750.

[137] Mock, S. A.; Sharp, S. E.; Stoner, T. R.; Radetic, M. J.; Zell, E. T.; Wang, R. G. CeO_2 nanorods-supported transition metal catalysts for CO oxidation. *J. Colloid Interface Sci.* **2016**, *466*, 261–267.

[138] Yang, W. T.; Wang, X.; Song, S. Y.; Zhang, H. J. Syntheses and applications of noble-metal-free CeO_2-based mixed-oxide nanocatalysts. *Chem* **2019**, *5*, 1743–1774.

[139] Li, Z. H.; Liu, Z. S.; Gao, G. Q.; Zhao, W. N.; Jiang, Y. J.; Tang, X.; Dai, S.; Qu, Z.; Yan, N. Q.; Ma, L. Enhanced catalytic oxidation reactivity over atomically dispersed Pt/CeO_2 catalysts by CO activation. *Environ. Sci. Technol.* **2024**, *58*, 12201–12211.

[140] Maurer, F.; Jelic, J.; Wang, J. J.; Gänzler, A.; Dolcet, P.; Wöll, C.; Wang, Y. M.; Studt, F.; Casapu, M.; Grunwaldt, J. D. Tracking the formation, fate and consequence for catalytic activity of Pt single sites on CeO_2. *Nat. Catal.* **2020**, *3*, 824–833.

[141] Yuan, K.; Guo, Y.; Lin, Q. L.; Huang, L.; Ren, J. T.; Liu, H. C.; Yan, C. H.; Zhang, Y. W. Size effect-tuned water gas shift reaction activity and pathway on ceria supported platinum catalysts. *J. Catal.* **2021**, *394*, 121–130.

[142] Spezzati, G.; Su, Y. Q.; Hofmann, J. P.; Benavidez, A. D.; DeLaRiva, A. T.; McCabe, J.; Datye, A. K.; Hensen, E. J. M. Atomically dispersed Pd–O species on CeO_2(111) as highly active sites for low-temperature CO oxidation. *ACS Catal.* **2017**, *7*, 6887–6891.

[143] Guo, L. W.; Du, P. P.; Fu, X. P.; Ma, C.; Zeng, J.; Si, R.; Huang, Y. Y.; Jia, C. J.; Zhang, Y. W.; Yan, C. H. Contributions of distinct gold species to catalytic reactivity for carbon monoxide oxidation. *Nat. Commun.* **2016**, *7*, 13481.

[144] Guo, Y.; Mei, S.; Yuan, K.; Wang, D. J.; Liu, H. C.; Yan, C. H.; Zhang, Y. W. Low-temperature CO_2 methanation over CeO_2-supported Ru single atoms, nanoclusters, and nanoparticles competitively tuned by strong metal-support interactions and H-spillover effect. *ACS Catal.* **2018**, *8*, 6203–6215.

[145] Van Deelen, T. W.; Hernández Mejía, C.; De Jong, K. P. Control of metal-support interactions in heterogeneous catalysts to enhance activity and selectivity. *Nat. Catal.* **2019**, *2*, 955–970.

[146] Otero, G. S.; Lustemberg, P. G.; Prado, F.; Ganduglia-Pirovano, M. V. Relative stability of near-surface oxygen vacancies at the CeO_2(111) surface upon zirconium doping. *J. Phys. Chem. C* **2020**, *124*, 625–638.

[147] Sudarsanam, P.; Mallesham, B.; Reddy, P. S.; Großmann, D.; Grünert, W.; Reddy, B. M. Nano-Au/CeO_2 catalysts for CO oxidation: Influence of dopants (Fe, La and Zr) on the physicochemical properties and catalytic activity. *Appl. Catal. B: Environ.* **2014**, *144*, 900–908.

[148] Xu, H. D.; Zhang, Z. H.; Liu, J. X.; Do-Thanh, C. L.; Chen, H.; Xu,

S. H.; Lin, Q. J.; Jiao, Y.; Wang, J. L.; Wang, Y. et al. Entropy-stabilized single-atom Pd catalysts via high-entropy fluorite oxide supports. *Nat. Commun.* **2020**, *11*, 3908.

[149] Liu, X.; Jia, S. F.; Yang, M.; Tang, Y. T.; Wen, Y. W.; Chu, S. Q.; Wang, J. B.; Shan, B.; Chen, R. Author correction: Activation of subnanometric Pt on Cu-modified CeO_2 via redox-coupled atomic layer deposition for CO oxidation. *Nat. Commun.* **2020**, *11*, 5879.

[150] Wang, C. L.; Gu, X. K.; Yan, H.; Lin, Y.; Li, J. J.; Liu, D. D.; Li, W. X.; Lu, J. L. Water-mediated Mars–van Krevelen mechanism for CO oxidation on ceria-supported single-atom Pt_1 catalyst. *ACS Catal.* **2017**, *7*, 887–891.

[151] Han, A. J.; Chen, W. X.; Zhang, S. L.; Zhang, M. L.; Han, Y. H.; Zhang, J.; Ji, S. F.; Zheng, L. R.; Wang, Y.; Gu, L. et al. A polymer encapsulation strategy to synthesize porous nitrogen-doped carbon-nanosphere-supported metal isolated-single-atomic-site catalysts. *Adv. Mater.* **2018**, *30*, 1706508.

[152] Lii-Rosales, A.; Han, Y.; Jing, D. P.; Tringides, M. C.; Julien, S.; Wan, K. T.; Wang, C. Z.; Lai, K. C.; Evans, J. W.; Thiel, P. A. Encapsulation of metal nanoparticles at the surface of a prototypical layered material. *Nanoscale* **2021**, *13*, 1485–1506.

[153] Gao, C. B.; Lyu, F.; Yin, Y. D. Encapsulated metal nanoparticles for catalysis. *Chem. Rev.* **2021**, *121*, 834–881.

[154] Elias, R. C.; Linic, S. Elucidating the roles of local and nonlocal rate enhancement mechanisms in plasmonic catalysis. *J. Am. Chem. Soc.* **2022**, *144*, 19990–19998.

[155] Schuurmans, J. H. A.; Masson, T. M.; Zondag, S. D. A.; Buskens, P.; Noël, T. Solar-driven continuous CO_2 reduction to CO and CH_4 using heterogeneous photothermal catalysts: Recent progress and remaining challenges. *ChemSusChem* **2024**, *17*, e202301405.

[156] Chuang, C. C.; Chu, H. C.; Huang, S. B.; Chang, W. S.; Tuan, H. Y. Laser-induced plasmonic heating in copper nanowire fabric as a photothermal catalytic reactor. *Chem. Eng. J.* **2020**, *379*, 122285.

[157] Ding, X.; Liu, W. X.; Zhao, J. H.; Wang, L.; Zou, Z. G. Photothermal CO_2 catalysis toward the synthesis of solar fuel: From material and reactor engineering to techno-economic analysis. *Adv. Mater.*, in press, DOI: 10.1002/adma.202312093.

[158] Olivo, A.; Ghedini, E.; Pascalicchio, P.; Manzoli, M.; Cruciani, G.; Signoretto, M. Sustainable carbon dioxide photoreduction by a cooperative effect of reactor design and titania metal promotion. *Catalysts* **2018**, *8*, 41.

[159] Cao, X. E.; Kaminer, Y.; Hong, T.; Schein, P.; Liu, T. W.; Hanrath, T.; Erickson, D. HI-light: A glass-waveguide-based "shell-and-tube" photothermal reactor platform for converting CO_2 to fuels. *iScience* **2020**, *23*, 101856.

[160] Wang, S. H.; Tountas, A. A.; Pan, W. B.; Zhao, J. J.; He, L.; Sun, W.; Yang, D. R.; Ozin, G. A. CO_2 footprint of thermal versus photothermal CO_2 catalysis. *Small* **2021**, *17*, 2007025.

[161] Fang, S. Y.; Hu, Y. H. Thermo-photo catalysis: A whole greater than the sum of its parts. *Chem. Soc. Rev.* **2022**, *51*, 3609–3647.

[162] Liu, Z. W.; Niu, L. J.; Zong, X. P.; An, L.; Qu, D.; Wang, X. Y.; Sun, Z. C. Ambient photothermal catalytic CO oxidation over a carbon-supported Palladium catalyst. *Appl. Catal. B: Environ.* **2022**, *313*, 121439.

[163] Bhatta, S.; Nagassou, D.; Mohsenian, S.; Trelles, J. P. Photo-thermochemical decomposition of carbon-dioxide in a direct solar receiver-reactor. *Solar Energy* **2019**, *178*, 201–214.

[164] Liu, X. Y.; Xing, C. S.; Yang, F.; Liu, Z.; Wang, Y. J.; Dong, T. J.; Zhao, L. L.; Liu, H.; Zhou, W. J. Strong interaction over Ru/defects-rich aluminium oxide boosts photothermal CO_2 methanation via microchannel flow-type system. *Adv. Energy Mater.* **2022**, *12*, 2201009.

[165] Fang, B. Z.; Xing, Y. L.; Bonakdarpour, A.; Zhang, S. C.; Wilkinson, D. P. Hierarchical CuO–TiO_2 hollow microspheres for highly efficient photodriven reduction of CO_2 to CH_4. *ACS Sustain. Chem. Eng.* **2015**, *3*, 2381–2388.

[166] Jantarang, S.; Lovell, E. C.; Tan, T. H.; Scott, J.; Amal, R. Role of support in photothermal carbon dioxide hydrogenation catalysed by Ni/$Ce_xTi_yO_2$. *Prog. Natl. Sci.: Mater. Int.* **2018**, *28*, 168–177.

[167] Vita, A.; Italiano, C.; Pino, L.; Laganà, M.; Ferraro, M.; Antonucci, V. High-temperature CO_2 methanation over structured Ni/GDC catalysts: Performance and scale-up for power-to-gas application. *Fuel Process. Technol.* **2020**, *202*, 106365.

[168] Azam, M. U.; Tahir, M.; Umer, M.; Jaffar, M. M.; Nawawi, M. G. M. Engineering approach to enhance photocatalytic water splitting for dynamic H_2 production using La_2O_3/TiO_2 nanocatalyst in a monolith photoreactor. *Appl. Surf. Sci.* **2019**, *484*, 1089–1101.

[169] Usubharatana, P.; McMartin, D.; Veawab, A.; Tontiwachwuthikul, P. Photocatalytic process for CO_2 emission reduction from industrial flue gas streams. *Ind. Eng. Chem. Res.* **2006**, *45*, 2558–2568.

[170] Khan, A. A.; Tahir, M. Recent advancements in engineering approach towards design of photo-reactors for selective photocatalytic CO_2 reduction to renewable fuels. *J. CO_2 Util.* **2019**, *29*, 205–239.

[171] Wei, L. F.; Yu, C. L.; Yang, K.; Fan, Q. Z.; Ji, H. B. Recent advances in VOCs and CO removal via photothermal synergistic catalysis. *Chin. J. Catal.* **2021**, *42*, 1078–1095.

[172] Qi, Y. H.; Jiang, J. W.; Liang, X. C.; Ouyang, S. X.; Mi, W. B.; Ning, S.; Zhao, L.; Ye, J. H. Fabrication of black In_2O_3 with dense oxygen vacancy through dual functional carbon doping for enhancing photothermal CO_2 hydrogenation. *Adv. Funct. Mater.* **2021**, *31*, 2100908.

[173] Kong, N.; Han, B.; Li, Z.; Fang, Y. S.; Feng, K.; Wu, Z. Y.; Wang, S. H.; Xu, A. B.; Yu, Y. Y.; Li, C. R. et al. Ruthenium nanoparticles supported on $Mg(OH)_2$ microflowers as catalysts for photothermal carbon dioxide hydrogenation. *ACS Appl. Nano Mater.* **2020**, *3*, 3028–3033.

[174] Fan, W. K.; Tahir, M. Recent developments in photothermal reactors with understanding on the role of light/heat for CO_2 hydrogenation to fuels: A review. *Chem. Eng. J.* **2022**, *427*, 131617.

[175] Song, C. Q.; Wang, Z. H.; Yin, Z.; Xiao, D. Q.; Ma, D. Principles and applications of photothermal catalysis. *Chem. Catal.* **2022**, *2*, 52–83.

[176] Qin, X. T.; Xu, M.; Guan, J. X.; Feng, L.; Xu, Y.; Zheng, L. R.; Wang, M.; Zhao, J. W.; Chen, J. L.; Zhang, J. et al. Direct conversion of CO and H_2O to hydrocarbons at atmospheric pressure using a TiO_{2-x}/Ni photothermal catalyst. *Nat. Energy* **2024**, *9*, 154–162.

[177] Jiang, H. Y.; Wang, L. Y.; Kaneko, H.; Gu, R. T.; Su, G. X.; Li, L.; Zhang, J.; Song, H. C.; Zhu, F.; Yamaguchi, A. et al. Light-driven CO_2 methanation over Au-grafted $Ce_{0.95}Ru_{0.05}O_2$ solid–solution catalysts with activities approaching the thermodynamic limit. *Nat. Catal.* **2023**, *6*, 519–530.

[178] Ezugwu, S.; Kazemian, S.; William Choi, D. Y.; Fanchini, G. Contactless near-field scanning thermoreflectance imaging. *Nanoscale* **2017**, *9*, 4097–4106.

[179] Kurbanova, B. A.; Mussabek, G. K.; Timoshenko, V. Y.; Lysenko, V.; Utegulov, Z. N. Photothermal effects and heat conduction in nanogranular Silicon films. *Nanomaterials* **2021**, *11*, 2379.

[180] Brites, C. D. S.; Lima, P. P.; Silva, N. J. O.; Millán, A.; Amaral, V. S.; Palacio, F.; Carlos, L. D. Thermometry at the nanoscale. *Nanoscale* **2012**, *4*, 4799–4829.

[181] Wang, D.; Koh, Y. R.; Kudyshev, Z. A.; Maize, K.; Kildishev, A. V.; Boltasseva, A.; Shalaev, V. M.; Shakouri, A. Spatial and temporal nanoscale plasmonic heating quantified by thermoreflectance. *Nano Lett.* **2019**, *19*, 3796–3803.

[182] Sivan, Y.; Baraban, J.; Un, I. W.; Dubi, Y. Comment on "quantifying hot carrier and thermal contributions in plasmonic photocatalysis". *Science* **2019**, *364*, eaaw9367.

[183] Jiang, K.; Siahrostami, S.; Akey, A. J.; Li, Y. B.; Lu, Z. Y.; Lattimer, J.; Hu, Y. F.; Stokes, C.; Gangishetty, M.; Chen, G. X. et al. Transition-metal single atoms in a graphene shell as active centers for highly efficient artificial photosynthesis. *Chem* **2017**, *3*, 950–960.

[184] Wei, Y. C.; Wu, X. X.; Zhao, Y. L.; Wang, L.; Zhao, Z.; Huang, X. T.; Liu, J. M.; Li, J. Efficient photocatalysts of TiO_2 nanocrystals-supported PtRu alloy nanoparticles for CO_2 reduction with H_2O: Synergistic effect of Pt-Ru. *Appl. Catal. B: Environ.* **2018**, *236*, 445–457.

[185] Gao, M. M.; Zhang, T. X.; Ho, G. W. Advances of photothermal chemistry in photocatalysis, thermocatalysis, and synergetic photothermocatalysis for solar-to-fuel generation. *Nano Res.* **2022**, *15*, 9985–10005.

[186] Toyao, T.; Kayamori, S.; Maeno, Z.; Siddiki, S. M. A. H.; Shimizu, K. I. Heterogeneous Pt and MoO_x Co-loaded TiO_2 catalysts for low-temperature CO_2 hydrogenation to form CH_3OH. *ACS Catal.* **2019**, *9*, 8187–8196.

[187] Xiong, Y.; Zhao, W. H.; Gu, D.; Tie, Z.; Zhang, W. H.; Jin, Z. Tunable C_2 products via photothermal steam reforming of CO_2 over surface-modulated mesoporous cobalt oxides. *Nano Lett.* **2023**, *23*, 4876–4884.

[188] Kattel, S.; Ramírez, P. J.; Chen, J. G.; Rodriguez, J. A.; Liu, P. Active sites for CO_2 hydrogenation to methanol on Cu/ZnO catalysts. *Science* **2017**, *355*, 1296–1299.

[189] Dai, B. C.; Cao, S. Q.; Xie, H. M.; Zhou, G. L.; Chen, S. M. Reduction of CO_2 to CO via reverse water-gas shift reaction over CeO_2 catalyst. *Korean J. Chem. Eng.* **2018**, *35*, 421–427.

[190] Liu, H. X.; Li, S. Q.; Wang, W. W.; Yu, W. Z.; Zhang, W. J.; Ma, C.; Jia, C. J. Partially sintered copper–ceria as excellent catalyst for the high-temperature reverse water gas shift reaction. *Nat. Commun.* **2022**, *13*, 867.

[191] Gu, D.; Jia, C. J.; Weidenthaler, C.; Bongard, H. J.; Spliethoff, B.; Schmidt, W.; Schüth, F. Highly ordered mesoporous cobalt-containing oxides: Structure, catalytic properties, and active sites in oxidation of carbon monoxide. *J. Am. Chem. Soc.* **2015**, *137*, 11407–11418.

[192] Zhao, J. Q.; Yang, Q.; Shi, R.; Waterhouse, G. I. N.; Zhang, X.; Wu, L. Z.; Tung, C. H.; Zhang, T. R. FeO–CeO_2 nanocomposites: An efficient and highly selective catalyst system for photothermal CO_2 reduction to CO. *NPG Asia Mater.* **2020**, *12*, 5.

[193] Deng, B. W.; Song, H.; Peng, K.; Li, Q.; Ye, J. H. Metal-organic framework-derived Ga-Cu/CeO_2 catalyst for highly efficient photothermal catalytic CO_2 reduction. *Appl. Catal. B: Environ.* **2021**, *298*, 120519.

[194] Jia, Z. W.; Ning, S. B.; Tong, Y. X.; Chen, X.; Hu, H. L.; Liu, L. Q.; Ye, J. H.; Wang, D. F. Selective photothermal reduction of CO_2 to CO over Ni-nanoparticle/N-doped CeO_2 nanocomposite catalysts. *ACS Appl. Nano Mater.* **2021**, *4*, 10485–10494.

[195] Lu, B. W.; Quan, F. J.; Sun, Z.; Jia, F. L.; Zhang, L. Z. Photothermal reverse-water-gas-shift over Au/CeO_2 with high yield and selectivity in CO_2 conversion. *Catal. Commun.* **2019**, *129*, 105724.

[196] Yang, Z.; Zeng, M.; Wang, K.; Yue, X. Y.; Chen, X.; Dai, W. X.; Fu, X. Z. Visible light-assisted thermal catalytic reverse water gas reaction over Cu-CeO_2: The synergistic of hot electrons and oxygen vacancies induced by LSPR effect. *Fuel* **2022**, *315*, 123186.

[197] Zhu, Z. H.; Zhou, J.; Li, Q. H.; Liu, Z. R.; Deng, Q. Y.; Zhou, Z. L.; Li, C. X.; Fu, L.; Zhou, J. C.; Li, H. N. et al. Preparation of heterostructured Cu-CeO_2/$SrTiO_3$ catalysts by rapid plasma exsolution for photothermal reverse water gas shift reaction. *J. CO_2 Util.* **2024**, *80*, 102665.

[198] Xiong, Y.; Liu, X.; Hu, Y.; Gu, D.; Jiang, M. H.; Tie, Z.; Jin, Z. $Ag_{24}Au$ cluster decorated mesoporous Co_3O_4 for highly selective and efficient photothermal CO_2 hydrogenation. *Nano Res.* **2022**, *15*, 4965–4972.

[199] Ashok, J.; Pati, S.; Hongmanorom, P.; Tianxi, Z.; Junmei, C.; Kawi, S. A review of recent catalyst advances in CO_2 methanation processes. *Catal. Today* **2020**, *356*, 471–489.

[200] Ulmer, U.; Dingle, T.; Duchesne, P. N.; Morris, R. H.; Tavasoli, A.; Wood, T.; Ozin, G. A. Fundamentals and applications of photocatalytic CO_2 methanation. *Nat. Commun.* **2019**, *10*, 3169.

[201] Ghaib, K.; Nitz, K.; Ben-Fares, F. Z. Chemical methanation of CO_2: A review. *ChemBioEng Rev.* **2016**, *3*, 266–275.

[202] Frontera, P.; Macario, A.; Ferraro, M.; Antonucci, P. Supported catalysts for CO_2 methanation: A review. *Catalysts* **2017**, *7*, 59.

[203] Zhang, K.; Xu, C. P.; Zhang, X. J.; Huang, Z. Y.; Pian, Q.; Che, K. H.; Cui, X. K.; Hu, Y. R.; Xuan, Y. M. Structural heredity in catalysis: CO_2 self-selective CeO_2 nanocrystals for efficient photothermal CO_2 hydrogenation to methane. *Small* **2024**, *23*, 2308823.

[204] Pan, D.; Wang, Y. N.; Li, H.; Zhang, Y. Z.; Liang, Q.; Zhou, M.; Li, Z. Y.; Xu, S. Solar light promoted CO_2 hydrogenation to CH_4 over photo-thermal responsive dispersed Co on defective CeO_2 composite derived from MOFs. *Sep. Purif. Technol.* **2024**, *332*, 125756.

[205] Fiorenza, R.; Bellardita, M.; Balsamo, S. A.; Spitaleri, L.; Gulino, A.; Condorelli, M.; D'Urso, L.; Scirè, S.; Palmisano, L. A solar photothermocatalytic approach for the CO_2 conversion: Investigation of different synergisms on CoO-CuO/brookite TiO_2-CeO_2 catalysts. *Chem. Eng. J.* **2022**, *428*, 131249.

[206] Yue, X. Y.; Wang, K.; Yang, Z.; Ni, W. K.; Zhang, Z. Z.; Dai, W. X.; Fu, X. Z. Visible light-regulated thermal catalytic selectivity induced by nonthermal effects over CuNi/CeO_2. *Chem. Eng. J.* **2023**, *458*, 141491.

[207] Bian, Z. F.; Chan, Y. M.; Yu, Y.; Kawi, S. Morphology dependence of catalytic properties of Ni/CeO_2 for CO_2 methanation: A kinetic and mechanism study. *Catal. Today* **2020**, *347*, 31–38.

[208] Siakavelas, G. I.; Charisiou, N. D.; AlKhoori, S.; AlKhoori, A. A.; Sebastian, V.; Hinder, S. J.; Baker, M. A.; Yentekakis, I. V.; Polychronopoulou, K.; Goula, M. A. Highly selective and stable nickel catalysts supported on ceria promoted with Sm_2O_3, Pr_2O_3 and MgO for the CO_2 methanation reaction. *Appl. Catal. B: Environ.* **2021**, *282*, 119562.

[209] Golovanova, V.; Spadaro, M. C.; Arbiol, J.; Golovanov, V.; Rantala, T. T.; Andreu, T.; Morante, J. R. Effects of solar irradiation on thermally driven CO_2 methanation using Ni/CeO_2-based catalyst. *Appl. Catal. B: Environ.* **2021**, *291*, 120038.

[210] Zhang, Z. Y.; Li, T.; Sun, X. L.; Luo, D. C.; Yao, J. L.; Yang, G. D.; Xie, T. Efficient photo-thermal catalytic CO_2 methanation and dynamic structural evolution over Ru/Mg-CeO_2 single-atom catalyst. *J. Catal.* **2024**, *430*, 115303.

[211] Tsiotsias, A. I.; Charisiou, N. D.; Yentekakis, I. V.; Goula, M. A. Bimetallic Ni-based catalysts for CO_2 methanation: A review. *Nanomaterials* **2020**, *11*, 28.

[212] Quindimil, A.; De-La-Torre, U.; Pereda-Ayo, B.; Davó-Quiñonero, A.; Bailón-García, E.; Lozano-Castelló, D.; González-Marcos, J. A.; Bueno-López, A.; González-Velasco, J. R. Effect of metal loading on the CO_2 methanation: A comparison between alumina supported Ni and Ru catalysts. *Catal. Today* **2020**, *356*, 419–432.

[213] Fu, G.; Jiang, M. H.; Liu, J.; Zhang, K. Q.; Hu, Y.; Xiong, Y.; Tao, A. Y.; Tie, Z.; Jin, Z. Rh/Al nanoantenna photothermal catalyst for wide-spectrum solar-driven CO_2 methanation with nearly 100% selectivity. *Nano Lett.* **2021**, *21*, 8824–8830.

[214] Li, Z. H.; Shi, R.; Zhao, J. Q.; Zhang, T. R. Ni-based catalysts derived from layered-double-hydroxide nanosheets for efficient photothermal CO_2 reduction under flow-type system. *Nano Res.* **2021**, *14*, 4828–4832.

[215] Xiong, Y.; Chen, H. W.; Hu, Y.; Yang, S. Y.; Xue, X. L.; He, L. F.; Liu, X.; Ma, J.; Jin, Z. Photodriven catalytic hydrogenation of CO_2 to CH_4 with nearly 100% selectivity over Ag_{25} clusters. *Nano Lett.* **2021**, *21*, 8693–8700.

[216] Bowker, M. Methanol synthesis from CO_2 hydrogenation. *ChemCatChem* **2019**, *11*, 4238–4246.

[217] Rodriguez, J. A.; Liu, P.; Stacchiola, D. J.; Senanayake, S. D.; White, M. G.; Chen, J. G. Hydrogenation of CO_2 to methanol: Importance of metal-oxide and metal-carbide interfaces in the activation of CO_2. *ACS Catal.* **2015**, *5*, 6696–6706.

[218] Jadhav, S. G.; Vaidya, P. D.; Bhanage, B. M.; Joshi, J. B. Catalytic carbon dioxide hydrogenation to methanol: A review of recent studies. *Chem. Eng. Res. Des.* **2014**, *92*, 2557–2567.

[219] Ren, M. H.; Zhang, Y. M.; Wang, X.; Qiu, H. S. Catalytic

hydrogenation of CO_2 to methanol: A review. *Catalysts* **2022**, *12*, 403.

[220] Fasihi, M.; Breyer, C. Global production potential of green methanol based on variable renewable electricity. *Energy Environ. Sci.* **2024**, *17*, 3503–3522.

[221] Yang, M.; Fan, D.; Wei, Y. X.; Tian, P.; Liu, Z. M. Recent progress in methanol-to-olefins (MTO) catalysts. *Adv. Mater.* **2019**, *31*, 1902181.

[222] IRENA. *Innovation Outlook: Renewable Methanol* [Online]. International Renewable Energy Agency: Abu Dhabi, 2021. https://www.irena.org/publications/2021/Jan/Innovation-Outlook-Renewable-Methanol (accessed Apr 20, 2024).

[223] Ganesh, I. Conversion of carbon dioxide into methanol—A potential liquid fuel: Fundamental challenges and opportunities (a review). *Renew. Sustain. Energy Rev.* **2014**, *31*, 221–257.

[224] Xie, B. Q.; Tan, T. H.; Kalantar-Zadeh, K.; Zheng, J. W.; Kumar, P.; Jiang, J. J.; Zhou, S. J.; Scott, J.; Amal, R. Promoting low-temperature methanol production over mixed oxide supported Cu catalysts: Coupling ceria-promotion and photo-activation. *Appl. Catal. B: Environ.* **2022**, *315*, 121599.

[225] Roode-Gutzmer, Q. I.; Kaiser, D.; Bertau, M. Renewable methanol synthesis. *ChemBioEng Rev.* **2019**, *6*, 209–236.

[226] Kanuri, S.; Roy, S.; Chakraborty, C.; Datta, S. P.; Singh, S. A.; Dinda, S. An insight of CO_2 hydrogenation to methanol synthesis: Thermodynamics, catalysts, operating parameters, and reaction mechanism. *Int. J. Energy Res.* **2022**, *46*, 5503–5522.

[227] Niu, J. T.; Liu, H. Y.; Jin, Y.; Fan, B. G.; Qi, W. J.; Ran, J. Y. Comprehensive review of Cu-based CO_2 hydrogenation to CH_3OH: Insights from experimental work and theoretical analysis. *Int. J. Hydrogen Energy* **2022**, *47*, 9183–9200.

[228] Dang, S. S.; Yang, H. Y.; Gao, P.; Wang, H.; Li, X. P.; Wei, W.; Sun, Y. H. A review of research progress on heterogeneous catalysts for methanol synthesis from carbon dioxide hydrogenation. *Catal. Today* **2019**, *330*, 61–75.

[229] Murthy, P. S.; Liang, W. B.; Jiang, Y. J.; Huang, J. Cu-based nanocatalysts for CO_2 hydrogenation to methanol. *Energy Fuels* **2021**, *35*, 8558–8584.

[230] Angelo, L.; Kobl, K.; Tejada, L. M. M.; Zimmermann, Y.; Parkhomenko, K.; Roger, A. C. Study of $CuZnMO_x$ oxides (M = Al, Zr, Ce, CeZr) for the catalytic hydrogenation of CO_2 into methanol. *Comptes Rendus. Chim.* **2015**, *18*, 250–260.

[231] Yoon, S.; Oh, K.; Liu, F. D.; Seo, J. H.; Somorjai, G. A.; Lee, J. H.; An, K. Specific metal-support interactions between nanoparticle layers for catalysts with enhanced methanol oxidation activity. *ACS Catal.* **2018**, *8*, 5391–5398.

[232] Wu, C. Y.; Cheng, D. Y.; Wang, M.; Ma, D. Understanding and application of strong metal-support interactions in conversion of CO_2 to methanol: A review. *Energy Fuels* **2021**, *35*, 19012–19023.

[233] Wang, W. W.; Qu, Z. P.; Song, L. X.; Fu, Q. CO_2 hydrogenation to methanol over Cu/CeO_2 and Cu/ZrO_2 catalysts: Tuning methanol selectivity via metal-support interaction. *J. Energy Chem.* **2020**, *40*, 22–30.

[234] Senanayake, S. D.; Ramírez, P. J.; Waluyo, I.; Kundu, S.; Mudiyanselage, K.; Liu, Z.; Liu, Z. Y.; Axnanda, S.; Stacchiola, D. J.; Evans, J. et al. Hydrogenation of CO_2 to methanol on CeO_x/Cu(111) and ZnO/Cu(111) catalysts: Role of the metal-oxide interface and importance of Ce^{3+} sites. *J. Phys. Chem. C* **2016**, *120*, 1778–1784.

[235] Ziemba, M.; Weyel, J.; Hess, C. Elucidating the mechanism of the reverse water-gas shift reaction over Au/CeO_2 catalysts using *operando* and transient spectroscopies. *Appl. Catal. B: Environ.* **2022**, *301*, 120825.

[236] Zhang, N. Q.; Miyazaki, S.; Qian, Y. C.; Jing, Y.; Toyao, T.; Shimizu, K. I. Mechanism of the periodic unsteady-state water-gas shift reaction on highly dispersed Cu-loaded CeO_2 catalysts. *ACS Catal.* **2023**, *13*, 8503–8515.

[237] Zhu, M. H.; Tian, P. F.; Cao, X. Y.; Chen, J. C.; Pu, T. C.; Shi, B. F.; Xu, J.; Moon, J.; Wu, Z. L.; Han, Y. F. Vacancy engineering of the nickel-based catalysts for enhanced CO_2 methanation. *Appl. Catal. B: Environ.* **2021**, *282*, 119561.

[238] Wang, F.; Wei, M.; Evans, D. G.; Duan, X. CeO_2-based heterogeneous catalysts toward catalytic conversion of CO_2. *J. Mater. Chem. A* **2016**, *4*, 5773–5783.

[239] Lange, J. P. Catalysis for biorefineries—Performance criteria for industrial operation. *Catal. Sci. Technol.* **2016**, *6*, 4759–4767.

[240] Kramm, U. I.; Marschall, R.; Rose, M. Pitfalls in heterogeneous thermal, electro- and photocatalysis. *ChemCatChem* **2019**, *11*, 2563–2574.

[241] Zhang, N. Q.; Li, L. C.; Jing, Y.; Qian, Y. C.; Chen, D. T.; Maeda, N.; Murayama, T.; Toyao, T.; Shimizu, K. I. *In situ*/*operando* spectroscopic evidence on associative redox mechanism for periodic unsteady-state water-gas shift reaction on Au/CeO_2 catalyst. *J. Catal.* **2024**, *433*, 115500.